Measurements in a water channel for studying environmental problems Part I

Fabien ANSELMET

IRPHE - Marseille

With : M. Amielh, O. Boiron, L. Pietri, A. Petroff, F. Ternat, (IRPHE)
P. Boyer, M.A. Gonze, A. Mailliat (CEA/IRSN, Cadarache)

- Introduction
- Water channel characteristic properties
- Cohesive sediment properties
- Aerosol dry deposition on vegetative canopies

Introduction

Water channel main advantages:

- large Reynolds numbers
- similitude with wind tunnels easily achieved

(especially for turbulent boundary layers: δ/x, $C_f = f(Re_x = U_e X/\nu)$)

- flow visualisations and LDV/PIV measurements easily performed

but non negligible acceleration effect when channel is long

(several to ten meters or more)

Water channel characteristic properties

Previous sediment experiments in the COM water channel

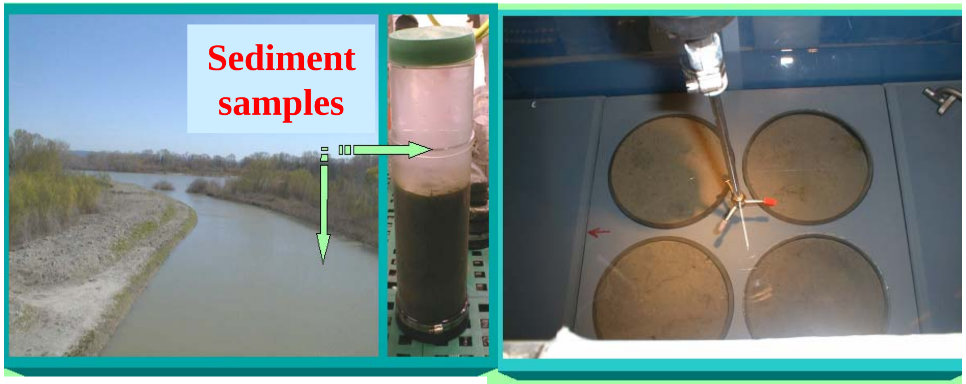

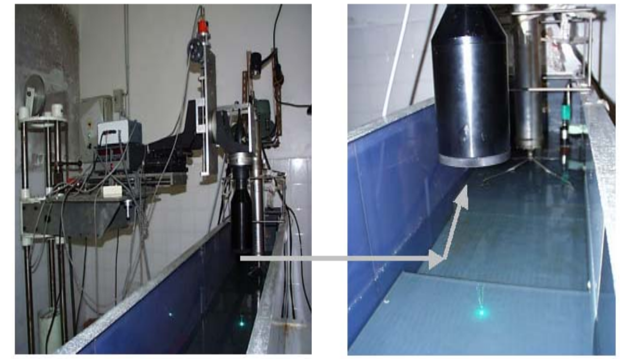

Water volume ≈ 2 to 4 m^3

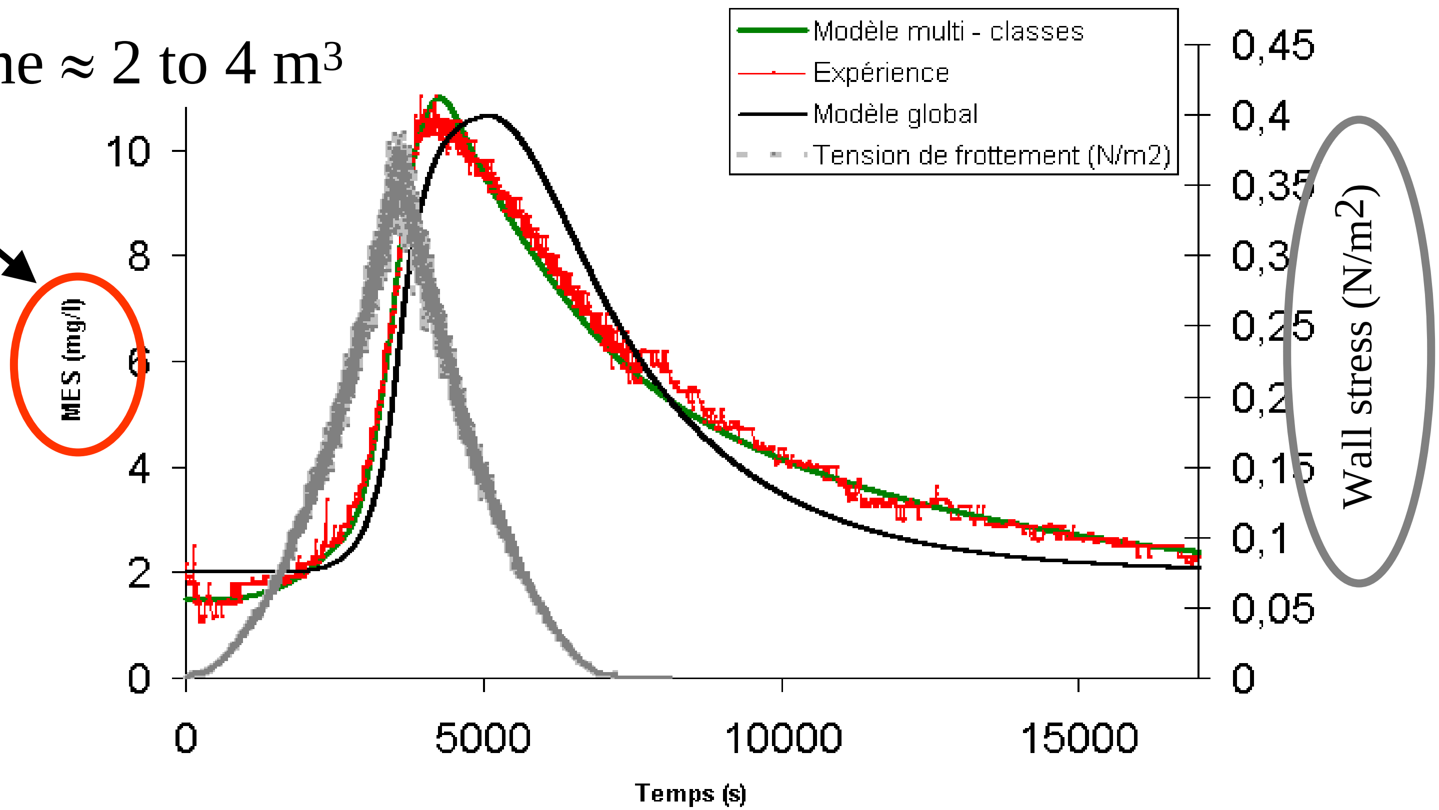

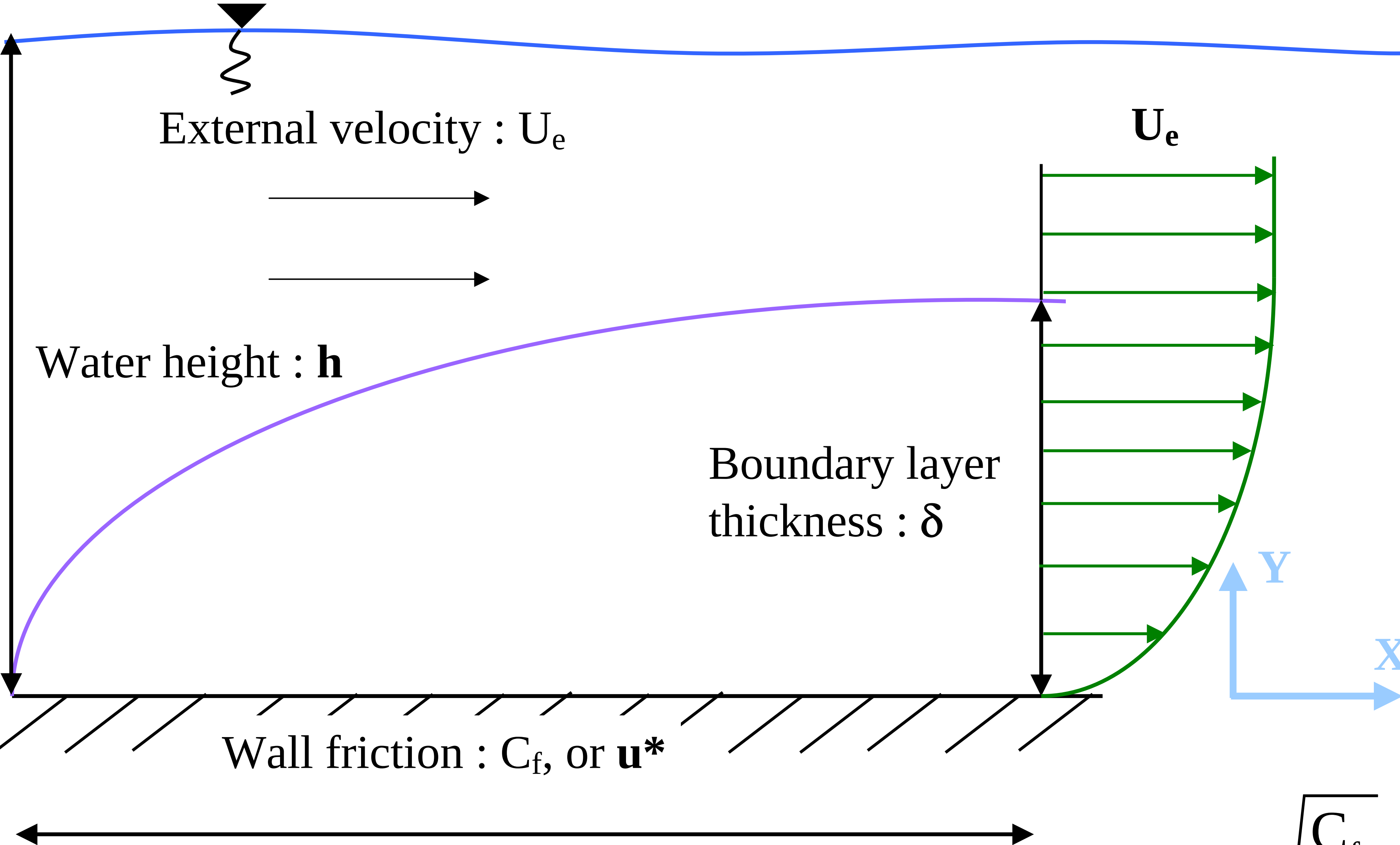

Development length : **X**

Spanwise dimension : **B**

$$u^* = U_e \sqrt{\frac{C_f}{2}}$$

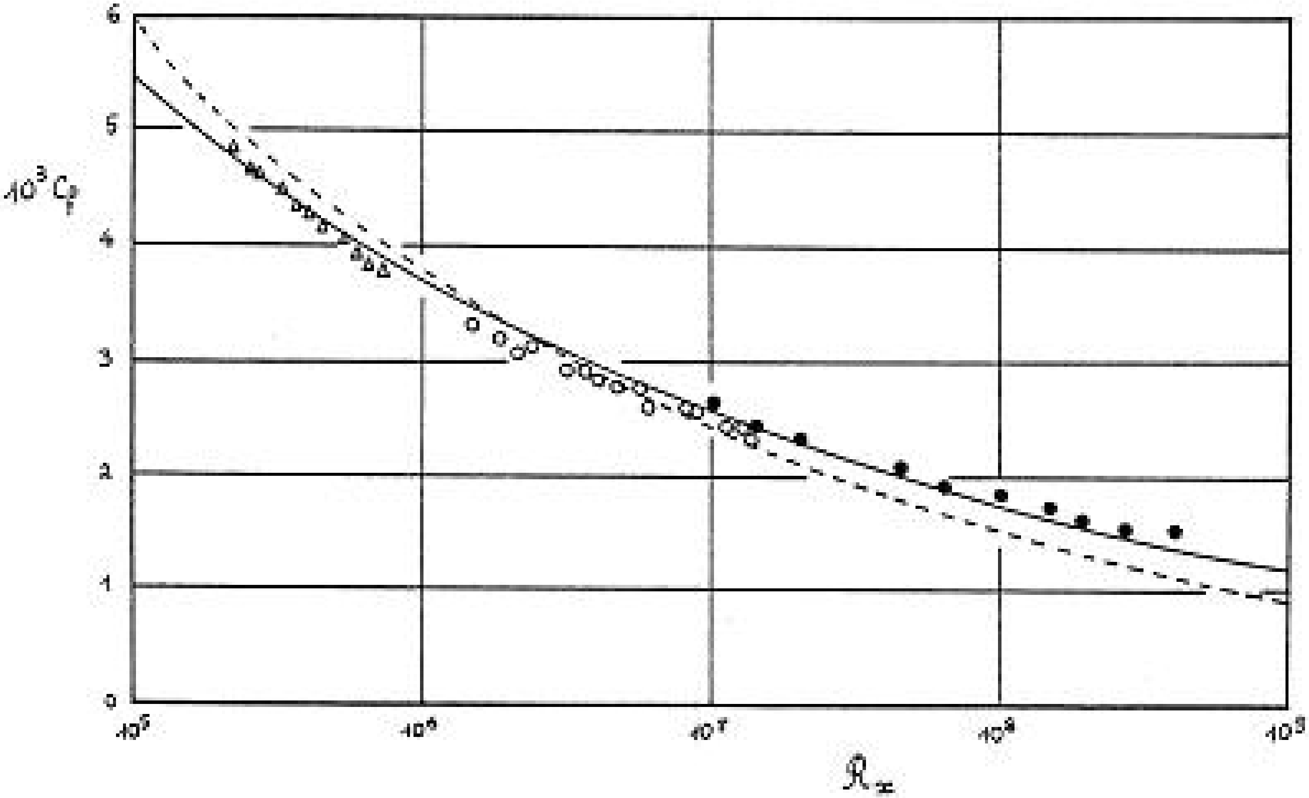

Fig. 7 - Coefficient de frottement de la plaque plane

------ $C_f = 0{,}0594 R_x^{-1/5}$ —— $C_f = 0{,}0368\ R_x^{-1/6}$

Résultats expérimentaux (regroupés par MICHEL)

Δ DHAWAN ○ SCHULTZ-GRUNOW ● KEMPF

$$Re_x = U_e . X / \nu$$

⇓

$$\delta/x = 0.38(Re_x)^{-1/5}$$

$$C_f = 0.059(Re_x)^{-1/5}$$

Wall stresses

$$\tau_p\ (=\rho u^{*2}) \leq 2\ Nm^{-2}$$

⇒

$$\begin{cases} U_e \approx 1 m/s \\ X \approx 1\ m \\ \delta \approx 3\ cm \end{cases}$$

Estimated boundary layer thicknesses (δ)

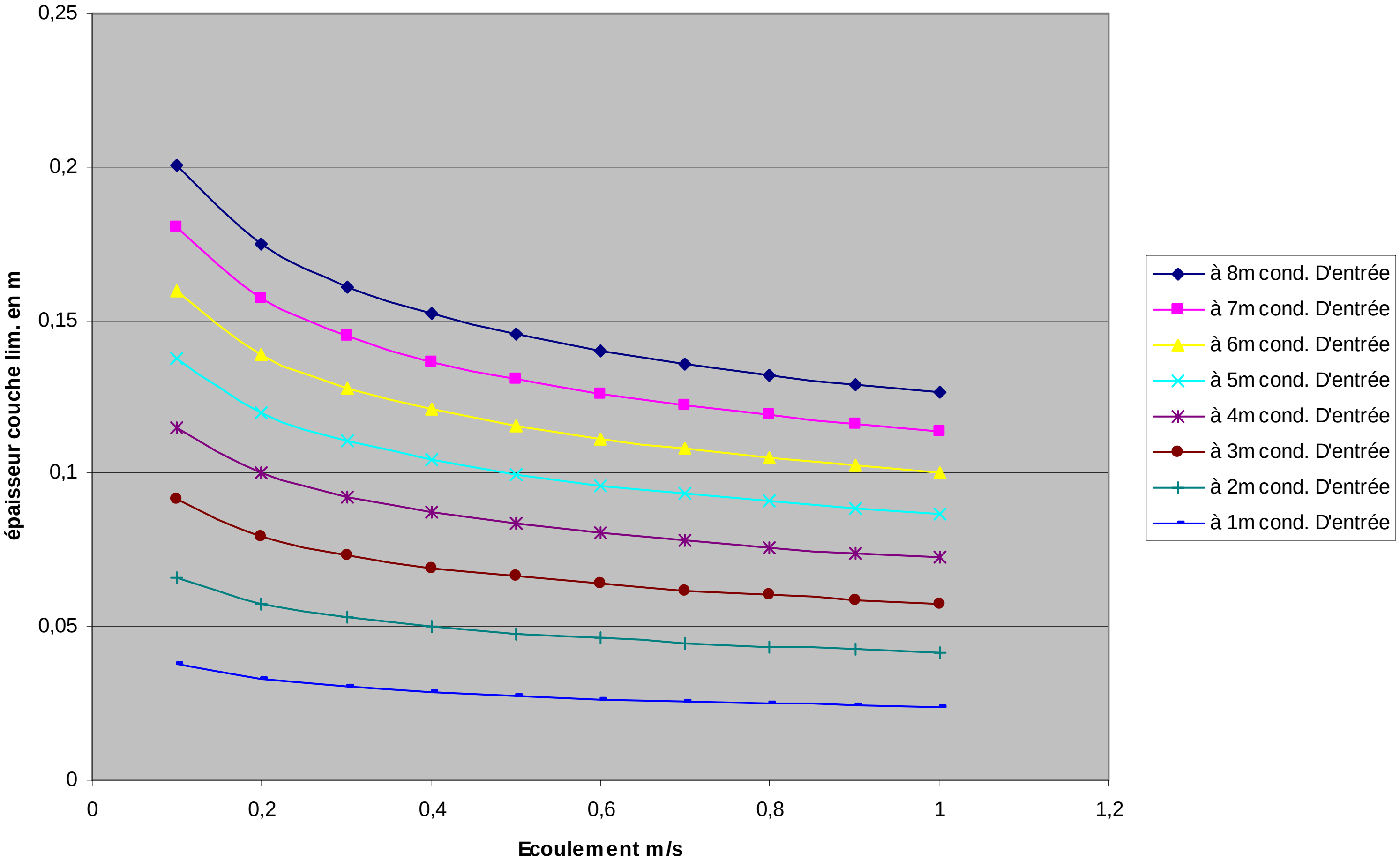

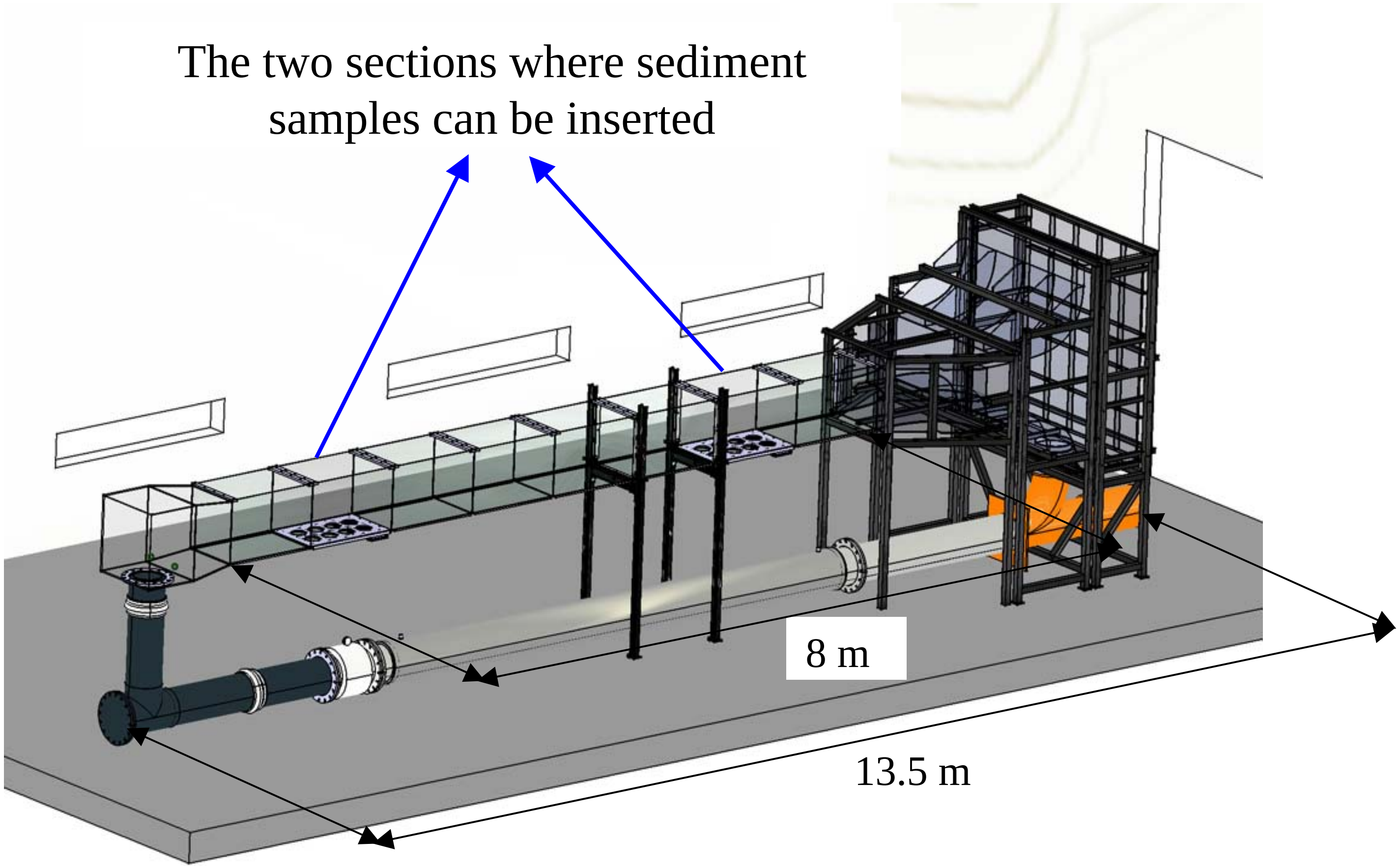

$B = 60$ cm, $10 \text{ cm} < h < 50$ cm, $0.1 \text{ m/s} < U_b < 1$ m/s

The water channel HERODE (built in 2003)

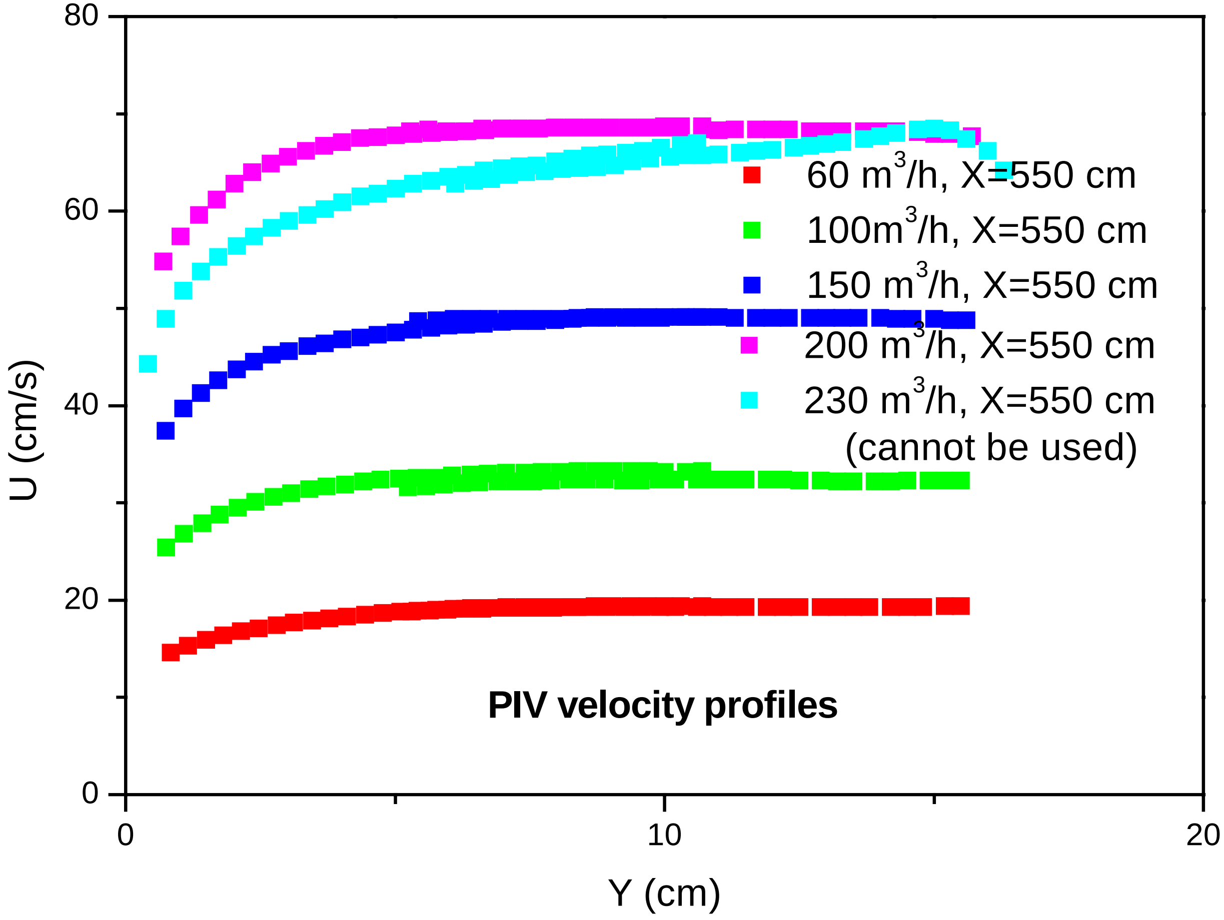

80
60
40
20
0
U (cm/s)
0
10
20
Y (cm)
60 m3/h, X=550 cm
100m3/h, X=550 cm
150 m3/h, X=550 cm
200 m3/h, X=550 cm
230 m3/h, X=550 cm
(cannot be used)
PIV velocity profiles

Bulk velocity : U_b

$$D_h = 4\frac{S}{P}$$

Side 'a' for a square duct
Diameter D for a circular pipe

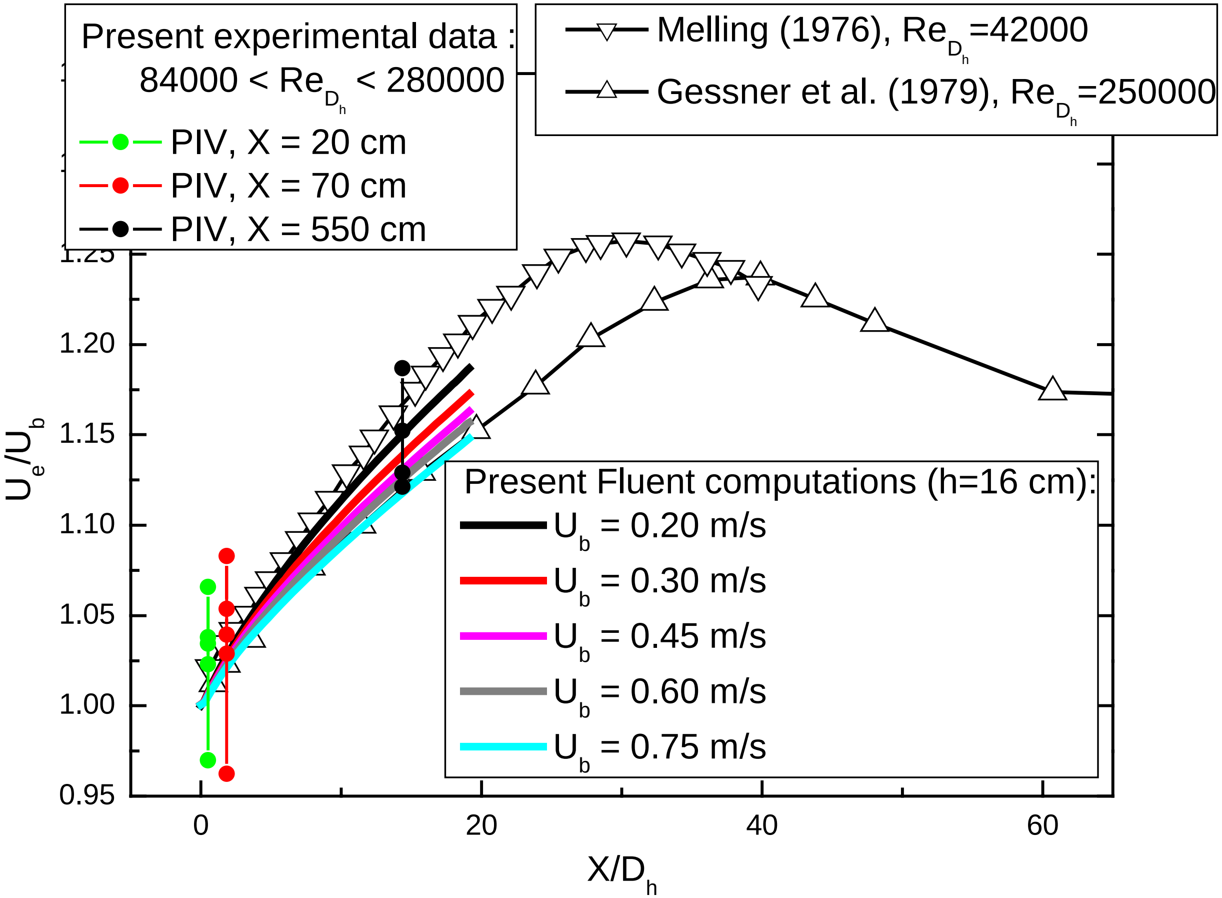

Any guideline for quantifying this acceleration effect ?

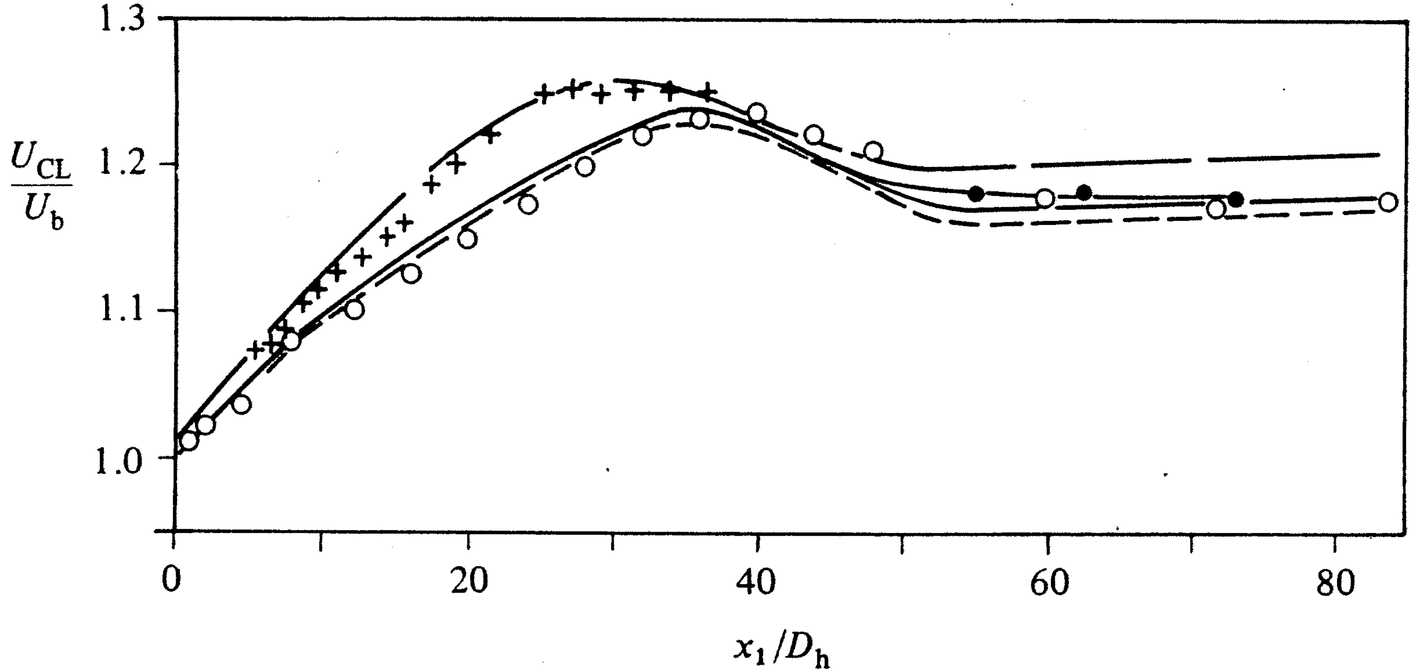

FIGURE 6. Flow development along axis of square duct. Data: +, Melling (1975), $Re = 42000$; ○, Gessner & Emery (1980), $Re = 250000$. Predictions: ——, present model, quadratic f-function, $Re = 50000$; —●—, present model, quadratic f-function, $Re = 250000$; ——, present model, linear f-function, $Re = 250000$; ---, model of Naot & Rodi (1982).

From Demuren and Rodi, JFM, 1984

For laminar conditions only, from White, ‘Viscous Fluid Flow’, 1991

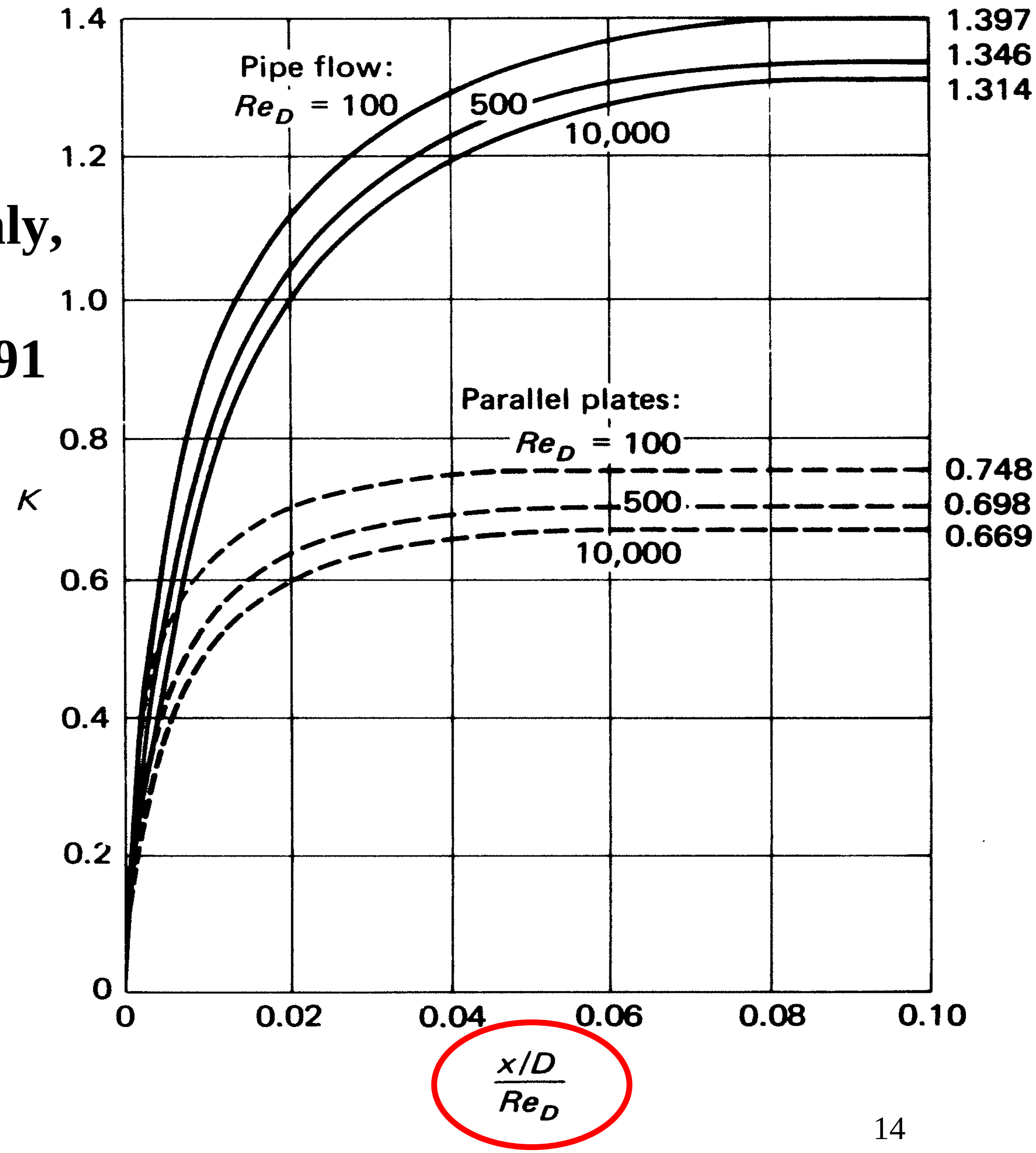

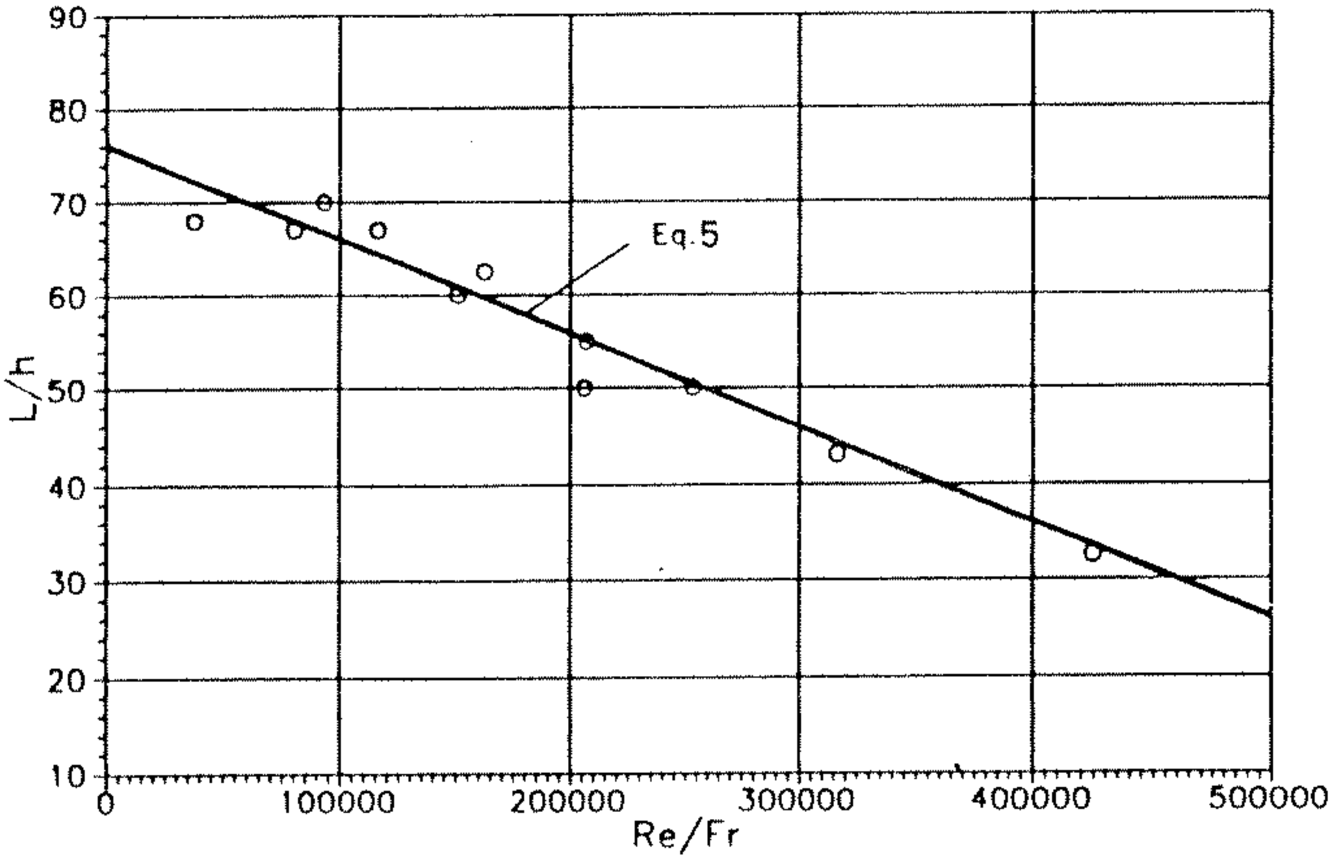

FIG. 3. Variation of Dimensionless Length of Flow Developing Zone with R/F

Data for open channels : only by Kirgöz and Ardichoglu (1997)

L/h = 76 –0.0001Re/Fr

For HERODE (h=16 cm) : L ≈ 4 m : wrong !!!

Our measurements for δ/x (with δ=h) suggest L ≈ 11 m

Need for a systematic study of the development region of pipe, duct and open channel flows

<u>3D Fluent computations :</u>

2 mesh sizes: ➔160x32x60 (8/24 m, 16 + 21 cm)
➔400x60x60 (40 m, 30 cm)
(+ circular pipe)

2 conditions for the « free surface »:
➔ zero friction (open channel)
➔ symmetry (square duct)

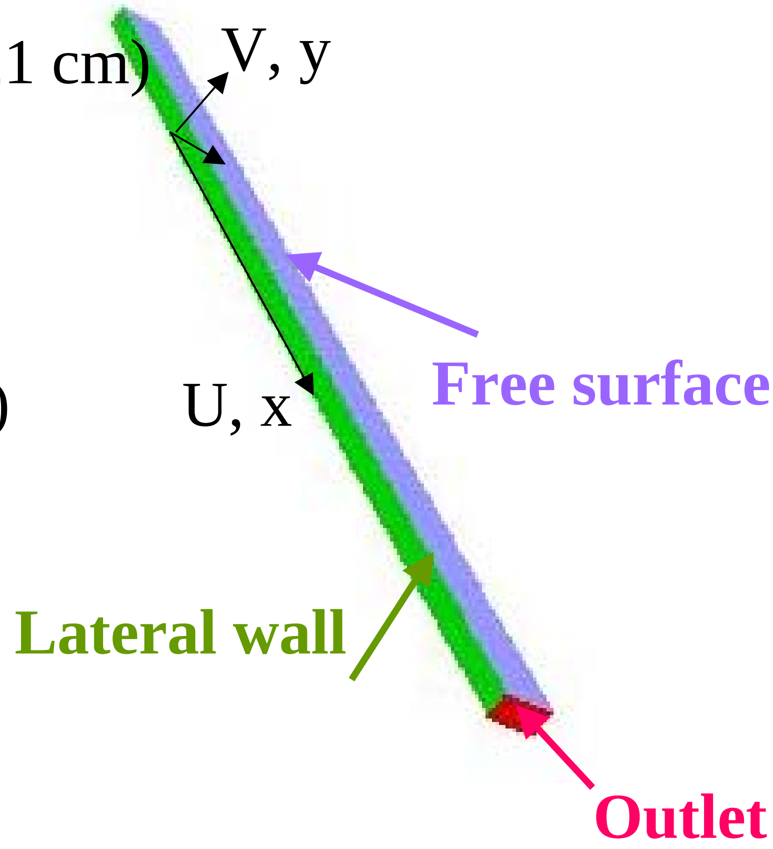

k-ε standard model :

(u_{rms} / U_b = 1%, $l \approx \frac{u_{rms}^3}{\varepsilon} = 1cm$: inlet)

Lengths : 8 m (stretched to 24 m) and 40 m

½ span (B) : 30 cm (with symmetry on the axis)

3 depths (h) : 16 cm, 21 cm, 30 cm

5 velocities : 20, 30, 45, 60 and 75 cm/s

	B (m)	h (m)	d = 2h (m)	D (m)	D_h (m)
Circular pipes				0.16, 0.21, 0.30	0.16, 0.21, 0.30
Ducts	0.60		0.32, 0.42, 0.60		0.418, 0.494, 0.60
Open-channels	0.60	0.16, 0.21, 0.30			0.418, 0.494, 0.60

Grid density	20x20	30x30	60x60	70x70
d^+_{1m}	64	26	2.5	1.1
d^+_{10m}	51	21	1.91	0.88

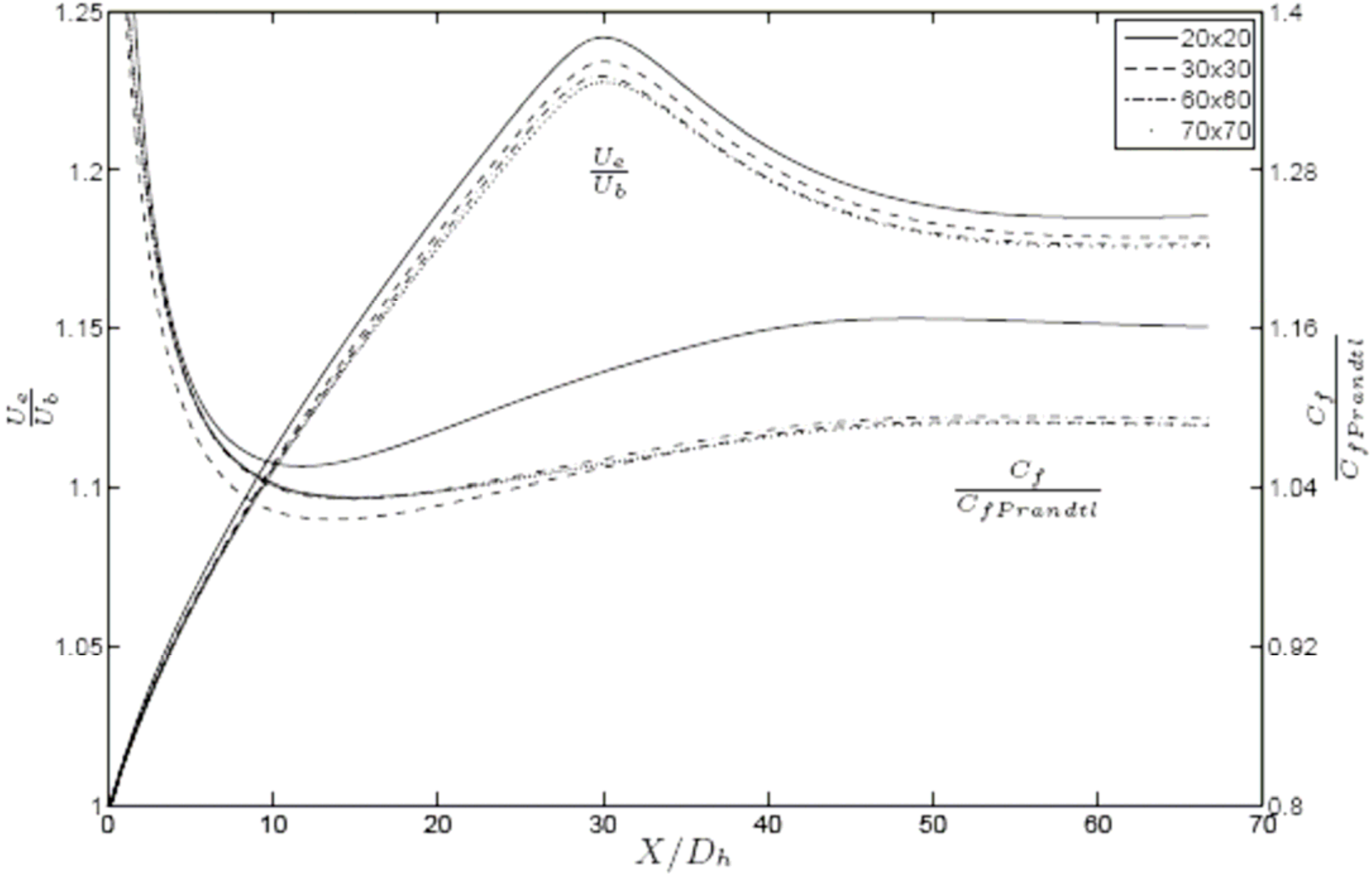

1.25
1.2
1.15
1.1
1.05
1
0
10
20
30
40
50
60
70
1.4
1.28
1.16
1.04
0.92
0.8
20x20
30x30
60x60
70x70
$\frac{U_e}{U_b}$
$\frac{C_f}{C_{f Prandtl}}$
X/D_h

Duct, d = 2h = 32 cm (small mesh)

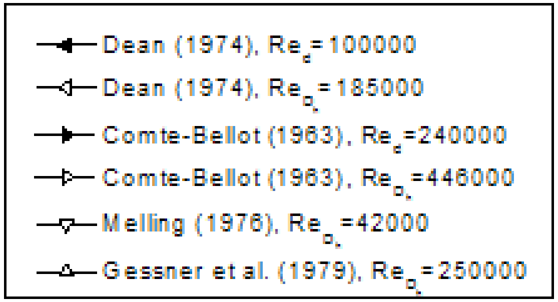

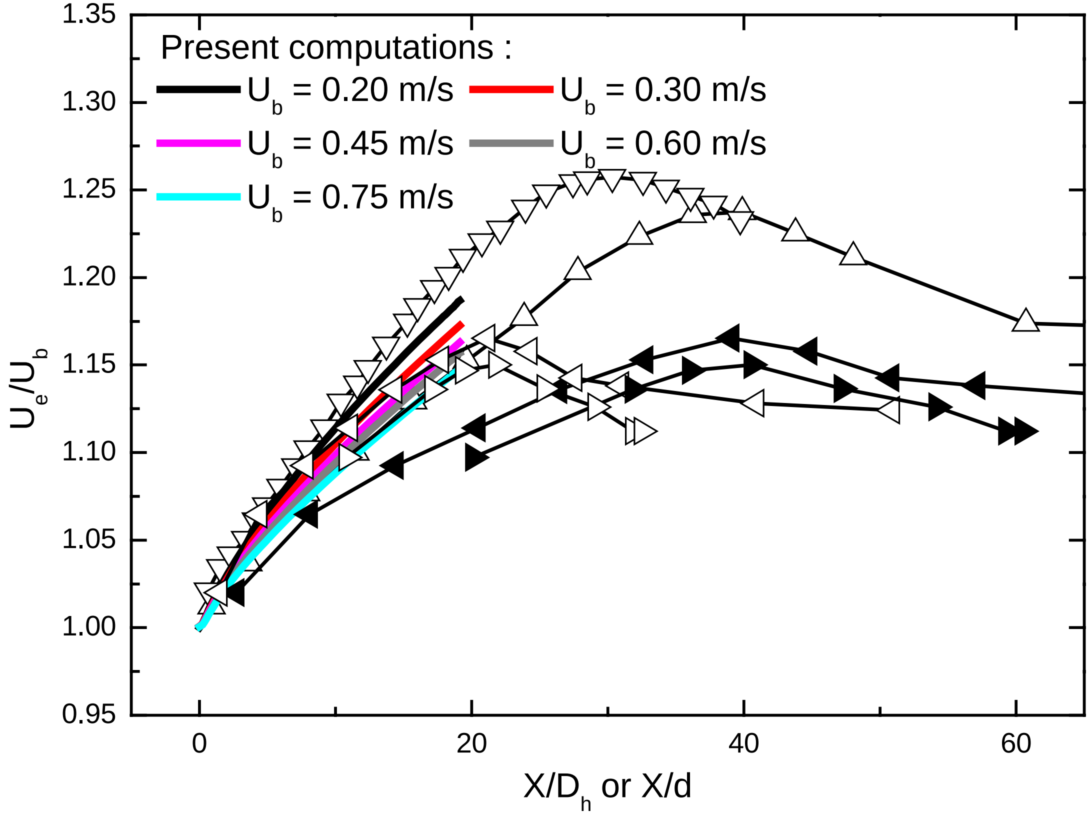

Duct, d = 2h = 32 cm (small mesh)

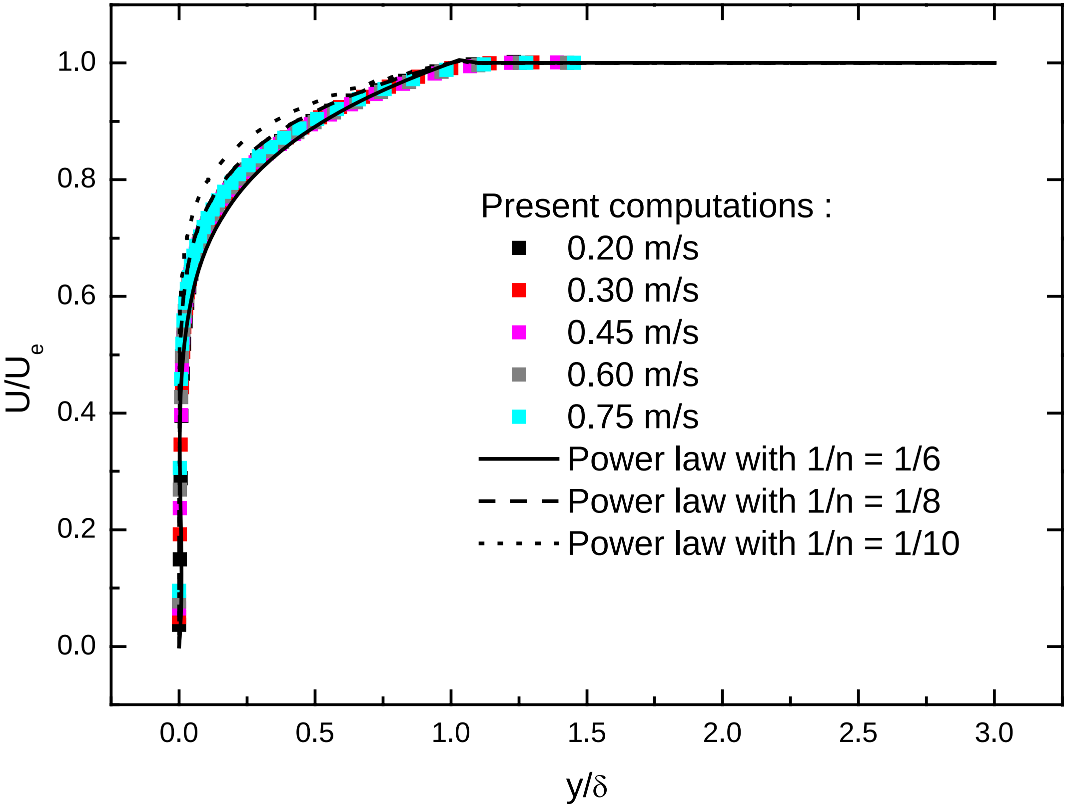

Duct, d = 2h = 60 cm (small mesh)

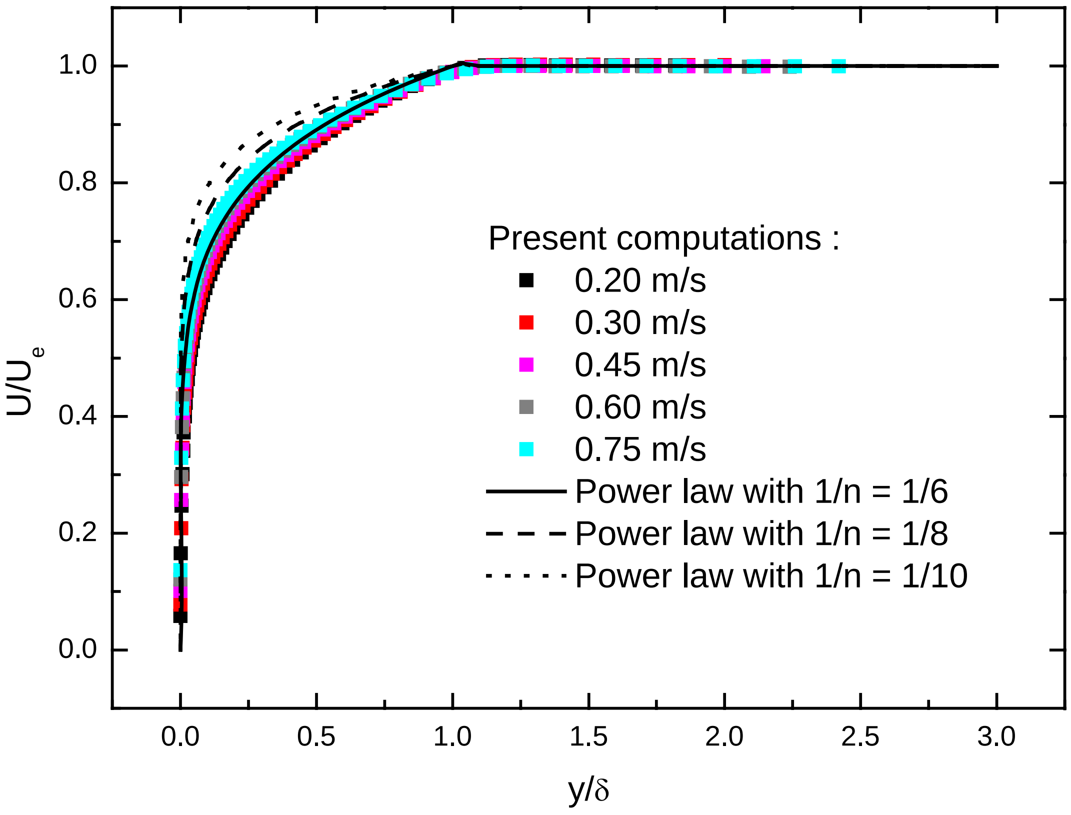

Duct, d = 2h = 32 cm (small mesh)

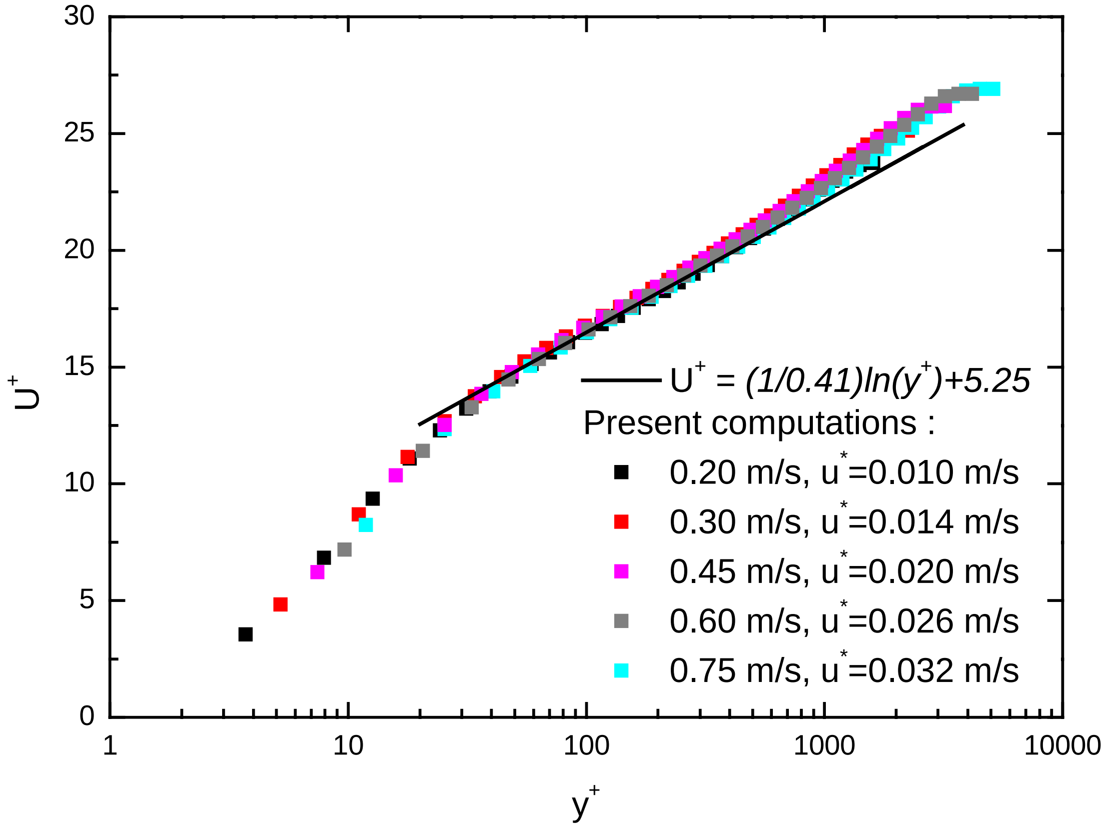

Duct, d = 2h = 60 cm (small mesh)

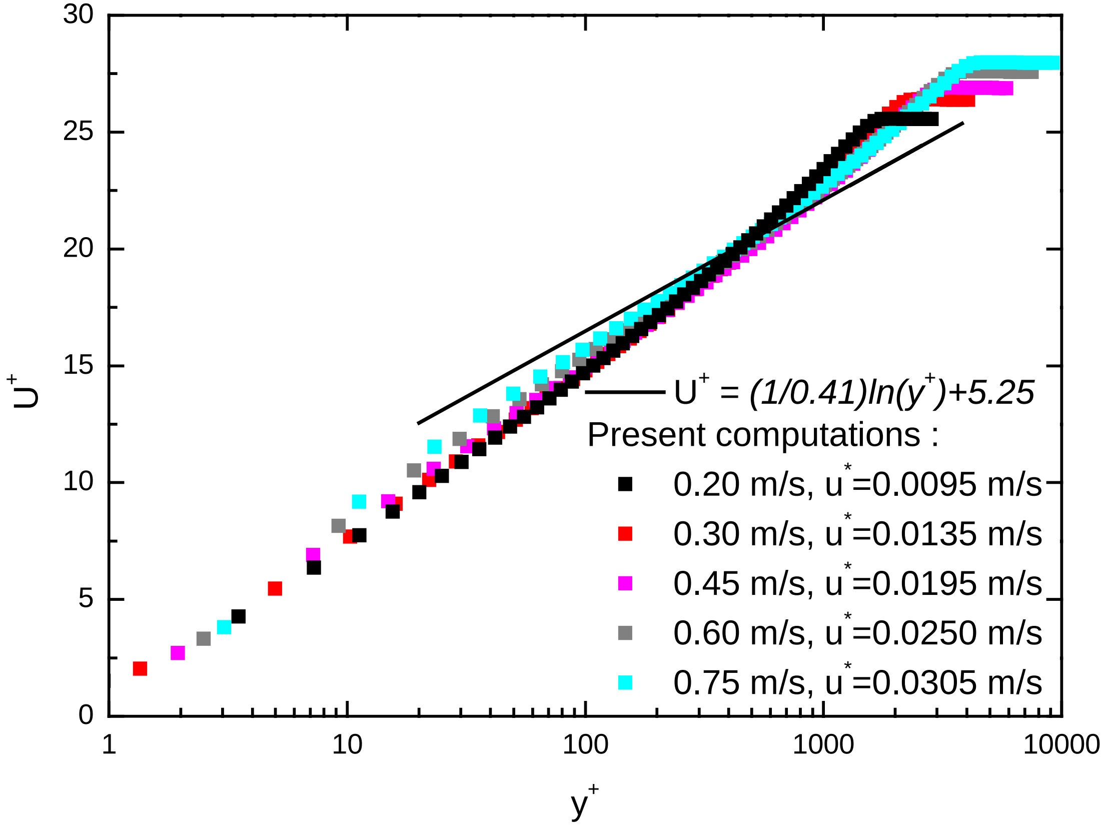

Schematic iso-velocity lines (experiments)

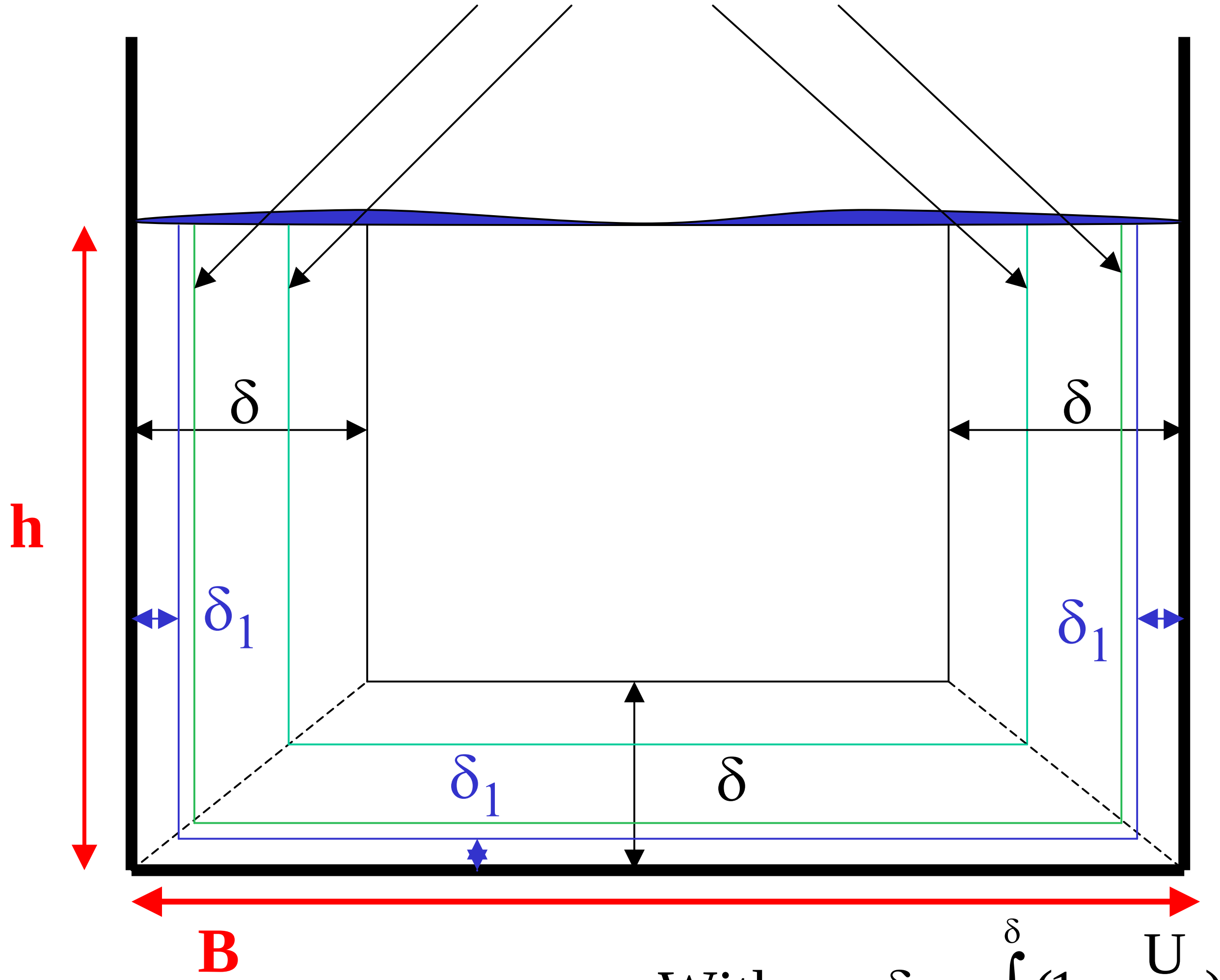

With : $\delta_1 = \int_0^{\delta} \left(1 - \frac{U}{U_e}\right) dy$

$$D_h = 4\frac{S}{P}\left(= 4\frac{Bh}{B+2h}\right)$$

For a velocity profile $U/Ue \approx (y/\delta)^{1/n}$,

$\delta_1 = \delta / (n+1)$

Circular pipes, D = 16 cm (■)   and D = 30 cm (☆)

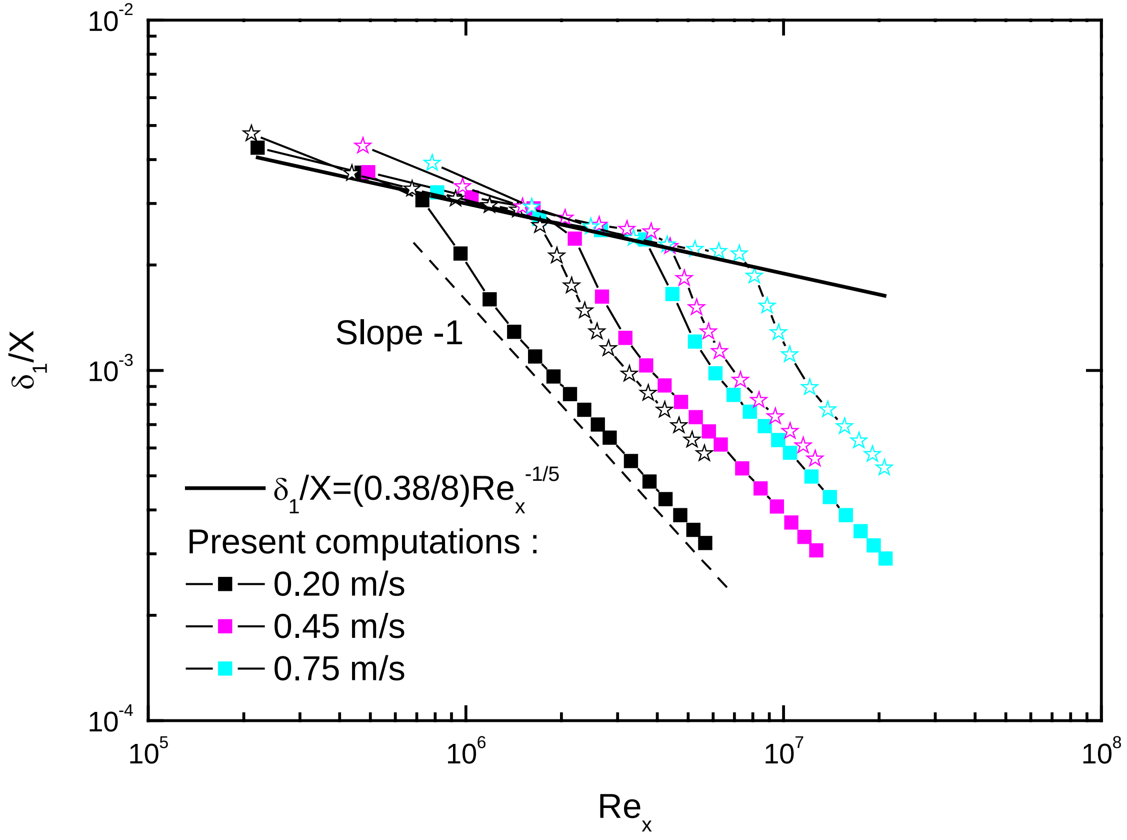

Square duct, d = 60 cm (■) and open channel h = 30 cm (☆)

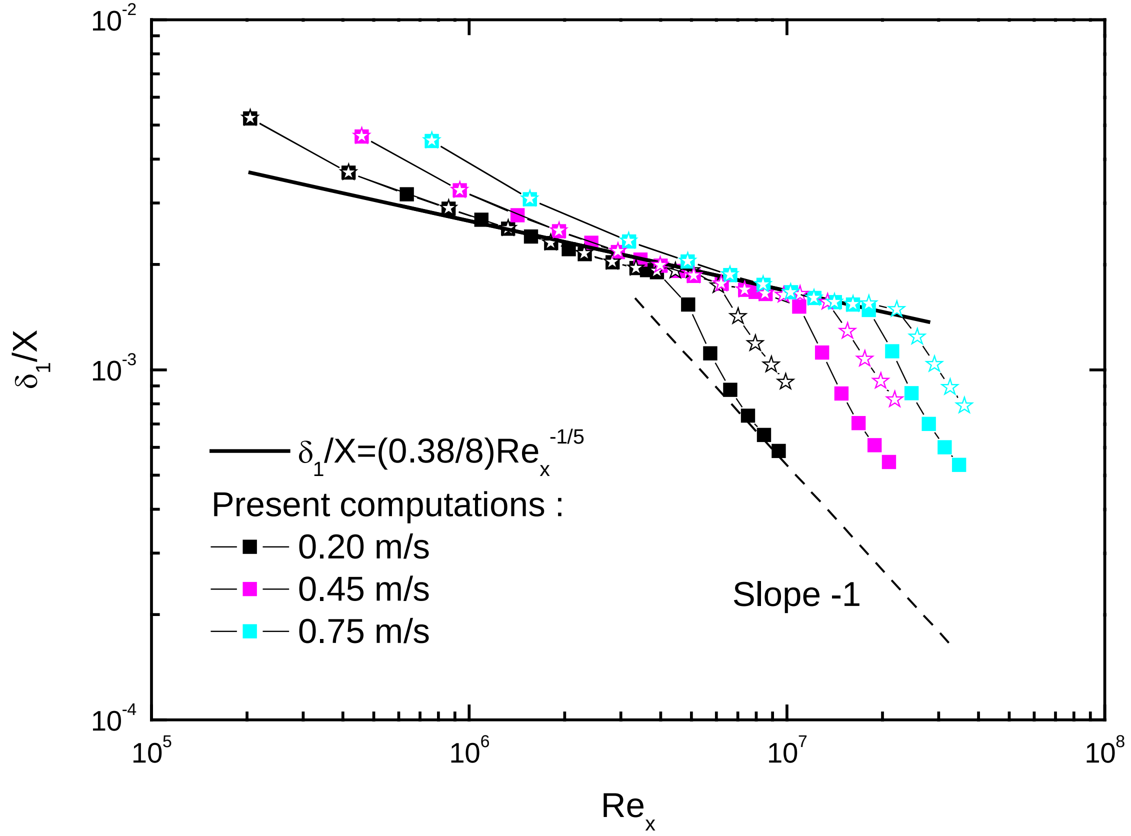

Influence of the acceleration ?

$$C_f = 2\frac{d\theta}{dx}, \quad \text{with } \theta = \int_0^\delta \frac{U}{U_e}\left(1-\frac{U}{U_e}\right)dy \quad \text{and} \quad H = \frac{\delta_1}{\theta} \approx 1 + 2/n \approx 1.3$$

$\Longrightarrow$ Slope for C_f = Slope for δ_1. (1/5).(n)/((n+1)(n+2))

if dU_e/dx negligible (≡(1/5).(7/72) with 1/n=1/7)

$$\text{but} \quad C_f = 2\frac{d\theta}{dx} - 2\theta\frac{H+2}{\rho U_e^2}\frac{dP}{dx} \quad \text{otherwise}$$

Circular pipes, D = 16 cm (———) and D = 30 cm (- · - ·)

Square duct, d = 60 cm (■) and open channel h = 30 cm (☆)

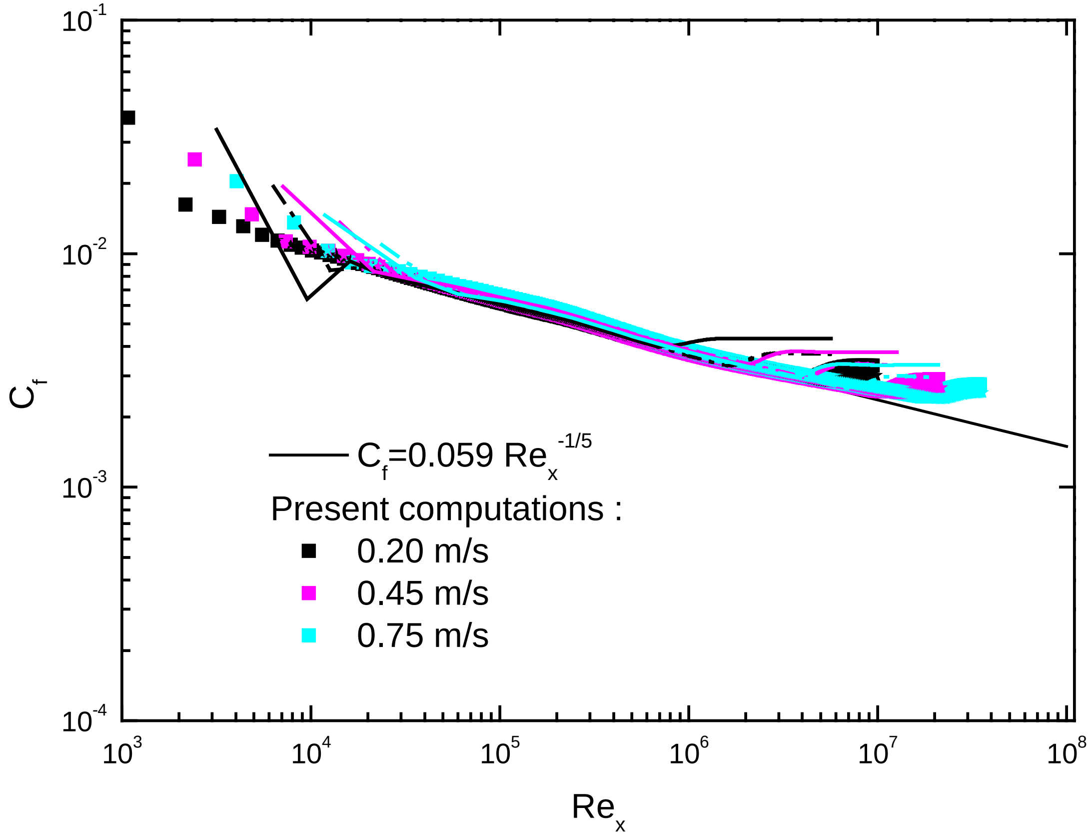

Circular pipes, D = 16 cm (——) and D = 30 cm (-·-·)

Square duct, d = 60 cm (■) and open channel h = 30 cm (☆)

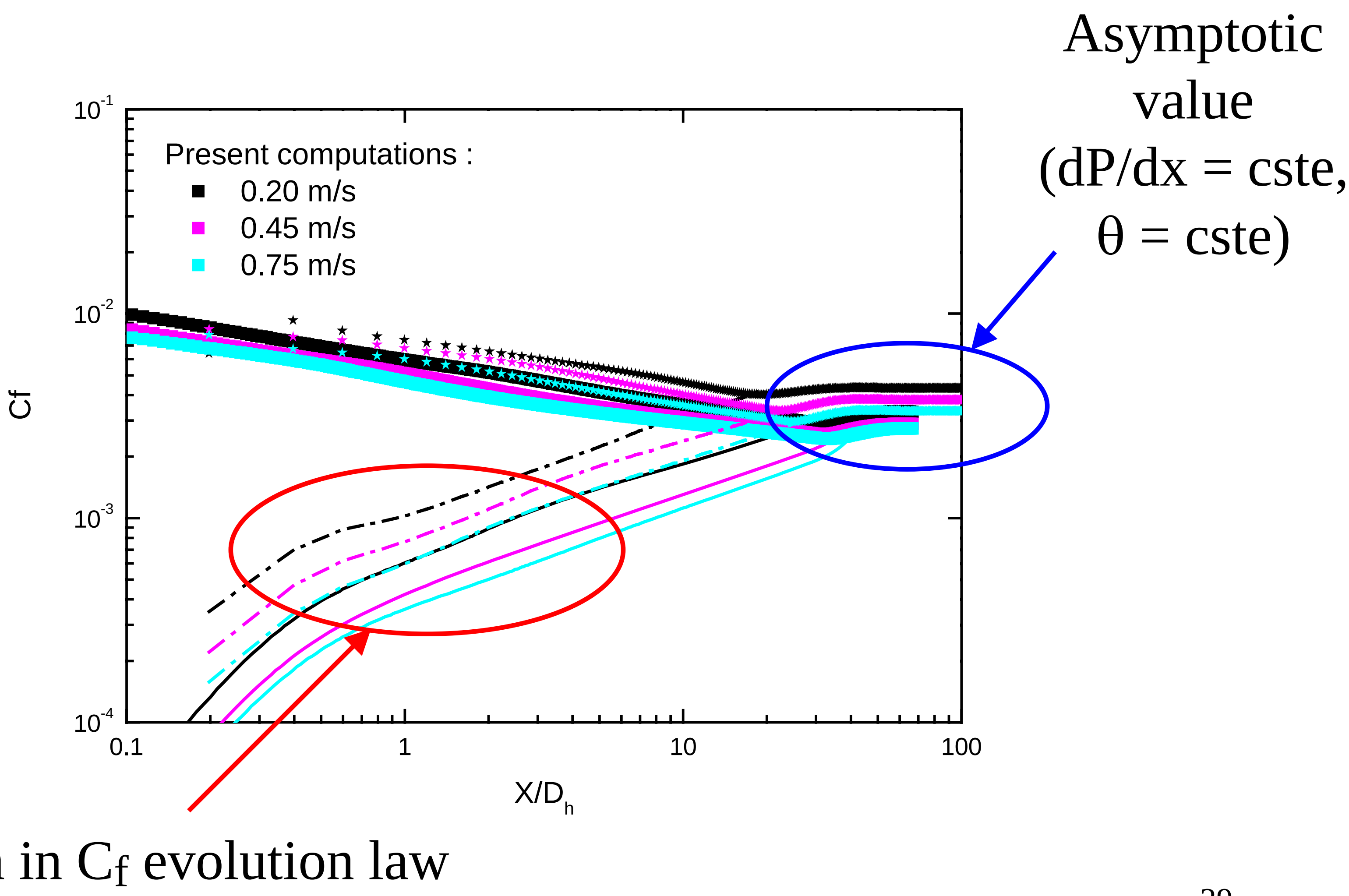

Circular pipes, D = 16 cm (———) and D = 30 cm (-·-·)

Rectangular duct, d = 32 cm (□) and open channel h = 16 cm (☆)

Square duct, d = 60 cm (■) and open channel h = 30 cm (★)

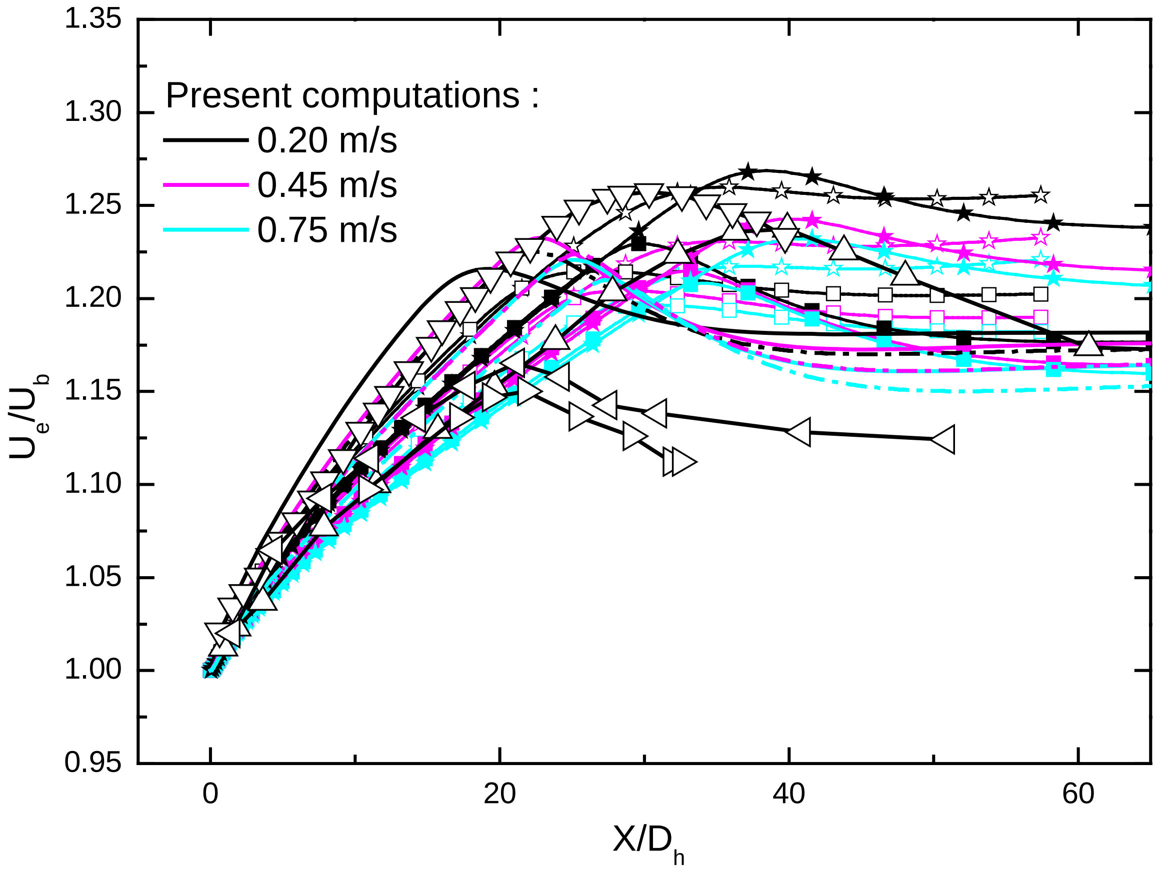

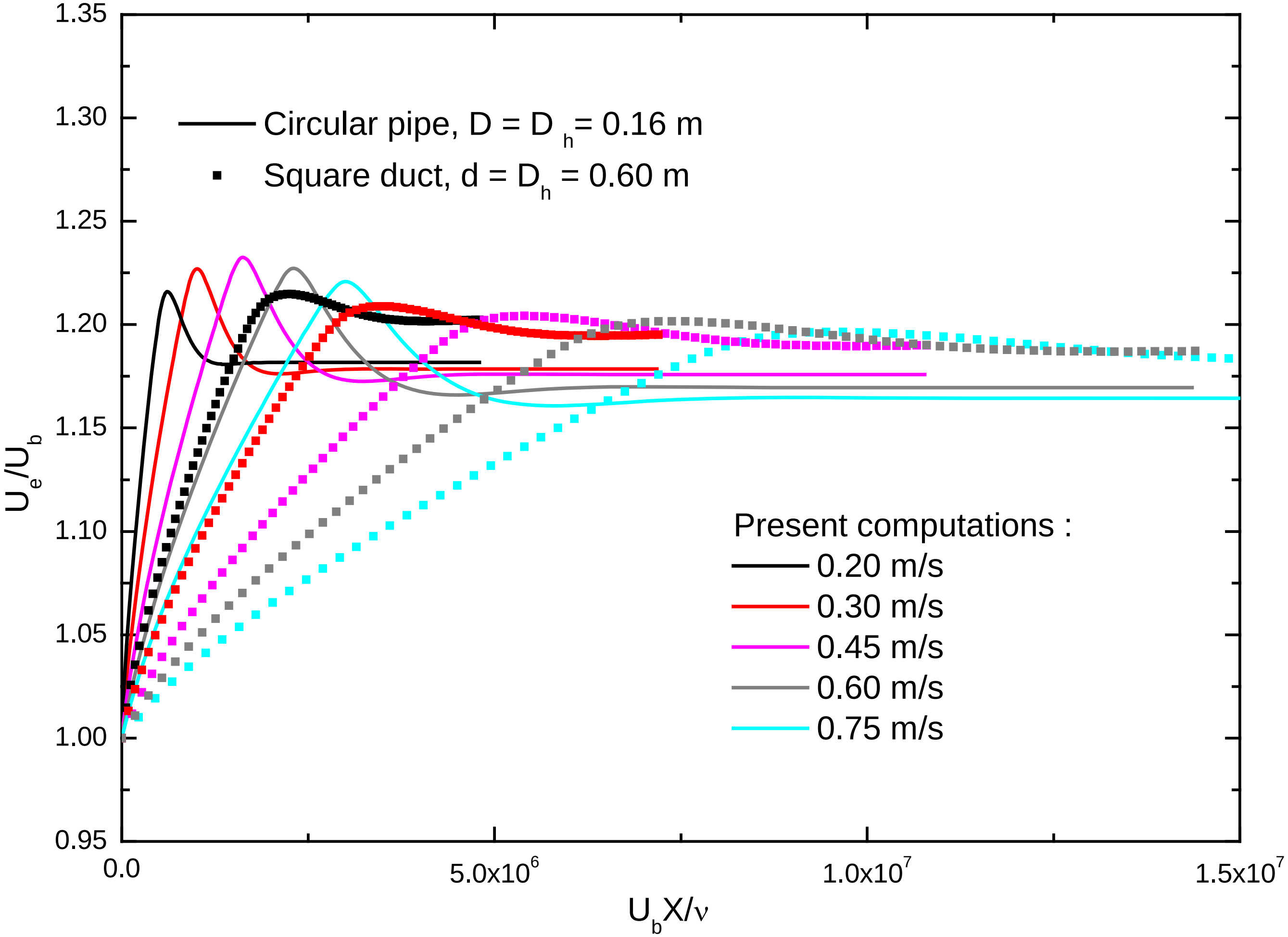

Circular pipe, D = D h= 0.16 m
Square duct, d = Dh = 0.60 m
Present computations :
0.20 m/s
0.30 m/s
0.45 m/s
0.60 m/s
0.75 m/s
1.35
1.30
1.25
1.20
1.15
1.10
1.05
1.00
0.95
Ue/Ub
0.0
5.0x10^6
1.0x10^7
1.5x10^7
UbX/ν

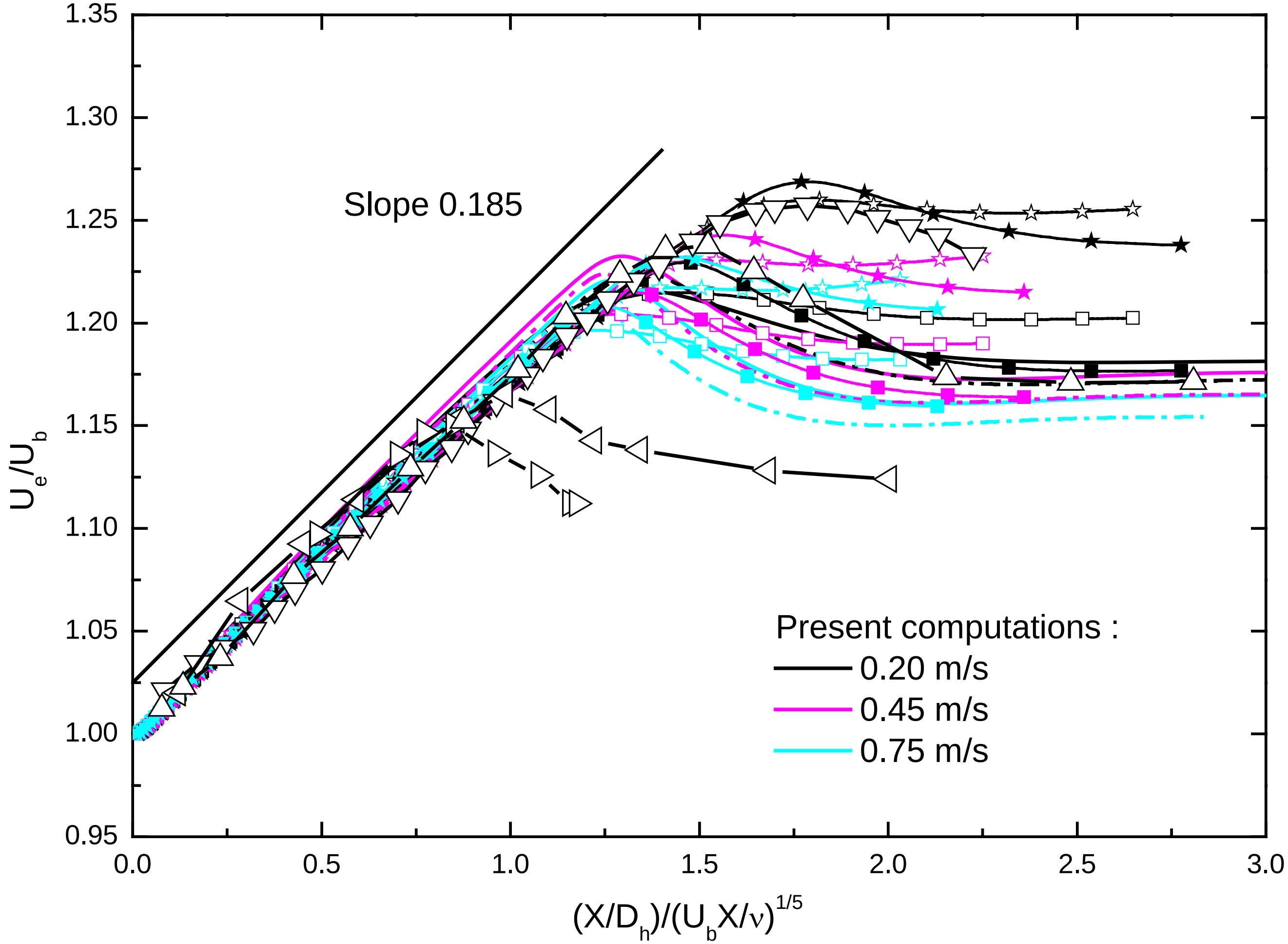

Slope 0.185
Present computations :
0.20 m/s
0.45 m/s
0.75 m/s
U_e/U_b
$(X/D_h)/(U_bX/\nu)^{1/5}$
1.35
1.30
1.25
1.20
1.15
1.10
1.05
1.00
0.95
0.0
0.5
1.0
1.5
2.0
2.5
3.0

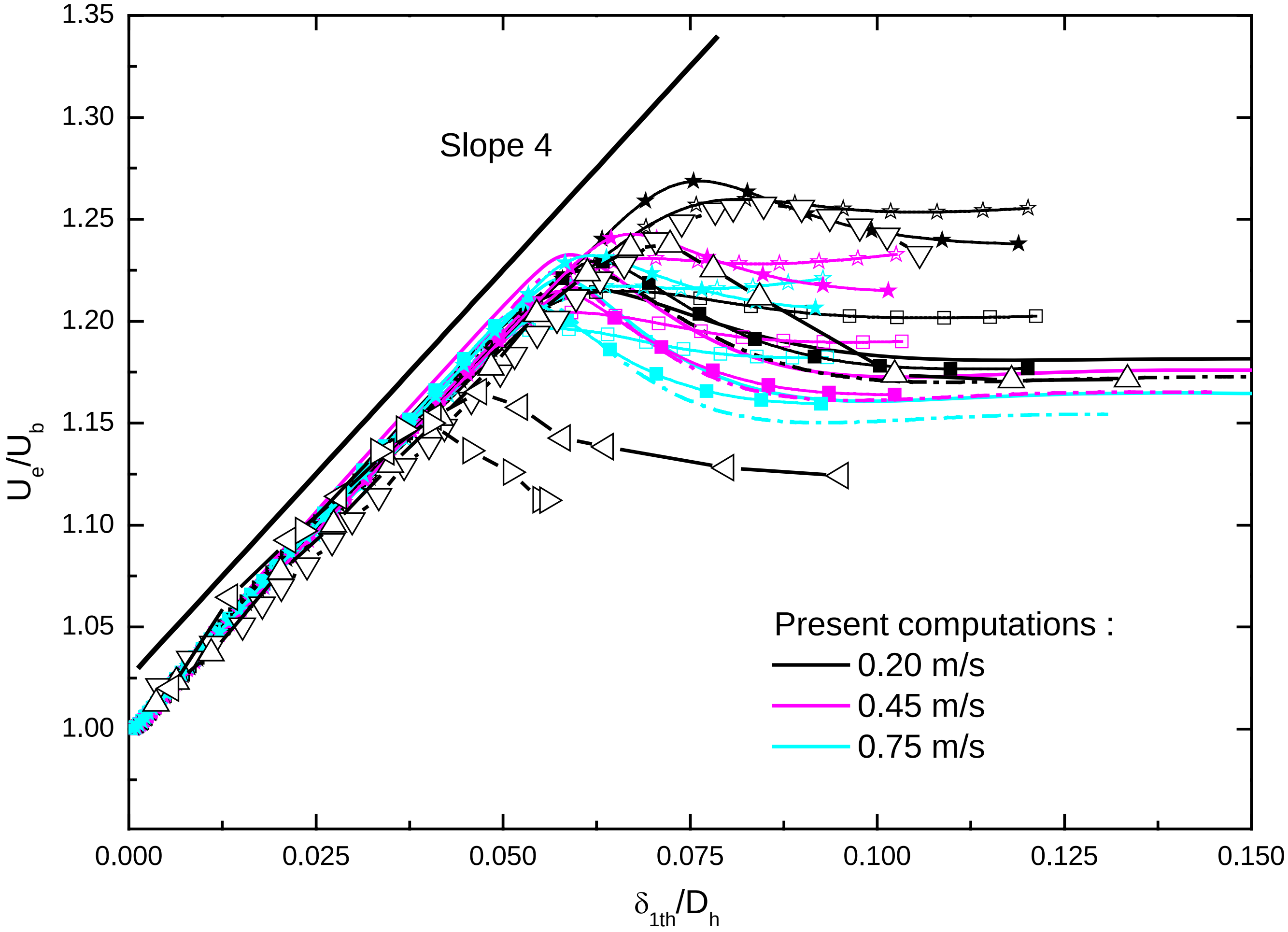

with $\delta_{1th} = (0.38/8) \times (Re_x)^{-1/5}$

(direct consequence of the flow rate conservation,
pipe flow : $U_b \frac{\pi}{4} D_h^2 = U_e \frac{\pi}{4}(D_h - 2\delta_1)^2, \quad \frac{U_e}{U_b} = \frac{1}{(1 - 2\delta_1/D_h)^2} \approx 1 + 4\delta_1/D_h$)

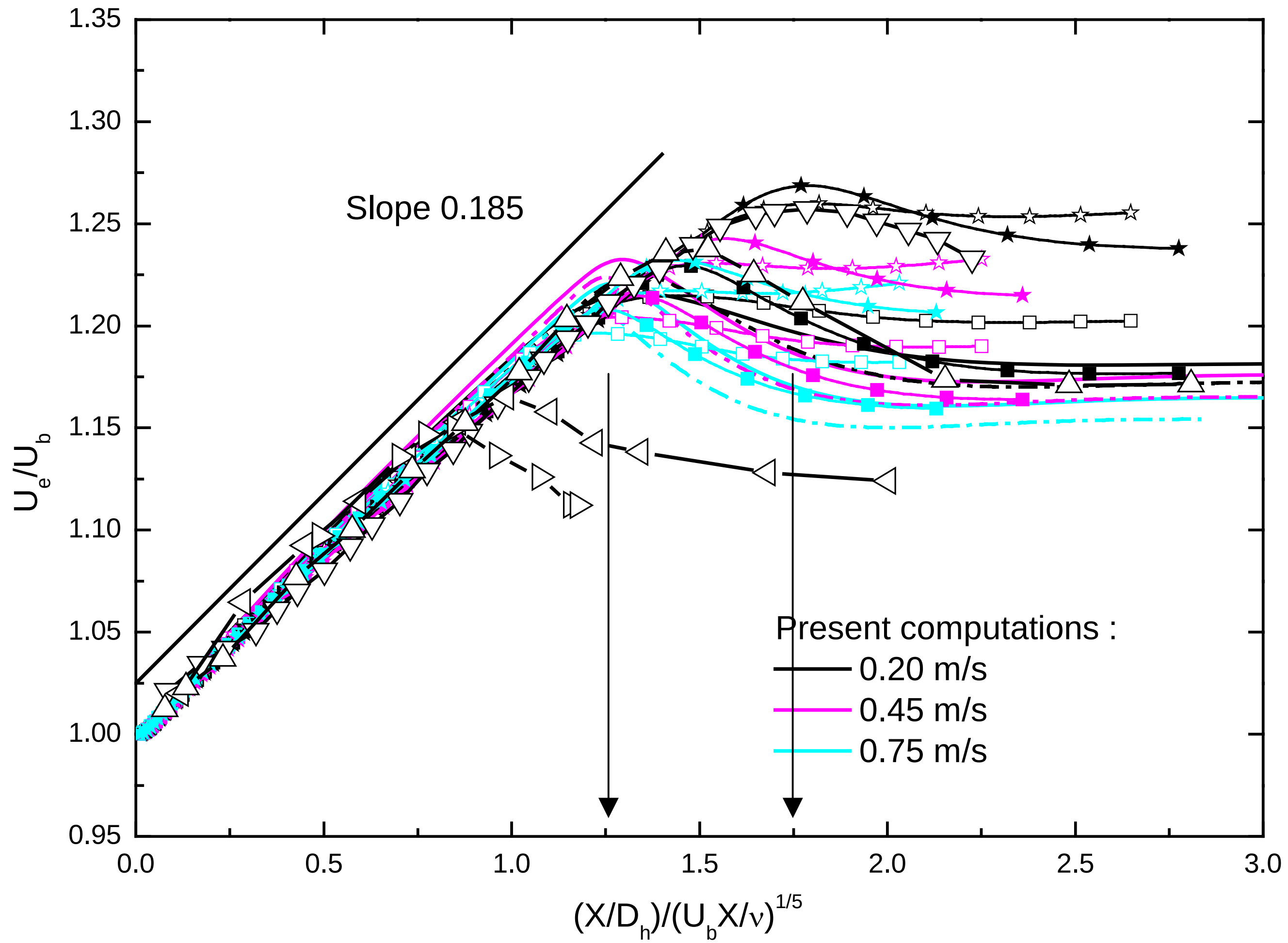

$$(X/D_h)/(U_b X/\nu)^{1/5} = C, \quad (L_e/D_h)^5 = C^5 U_b L_e/\nu$$

$$\boxed{L_e/D_h = C^{5/4}(U_b D_h/\nu)^{1/4} = C^{5/4}(Re)^{1/4}}\ , \qquad L_e/D_h = 1.3\,(Re)^{1/4}$$

or $2.0\,(Re)^{1/4}$

Szablewski (1953) : pipe flows, ★

Kirgöz and Ardichoglu (1997) : open channel flows, ○

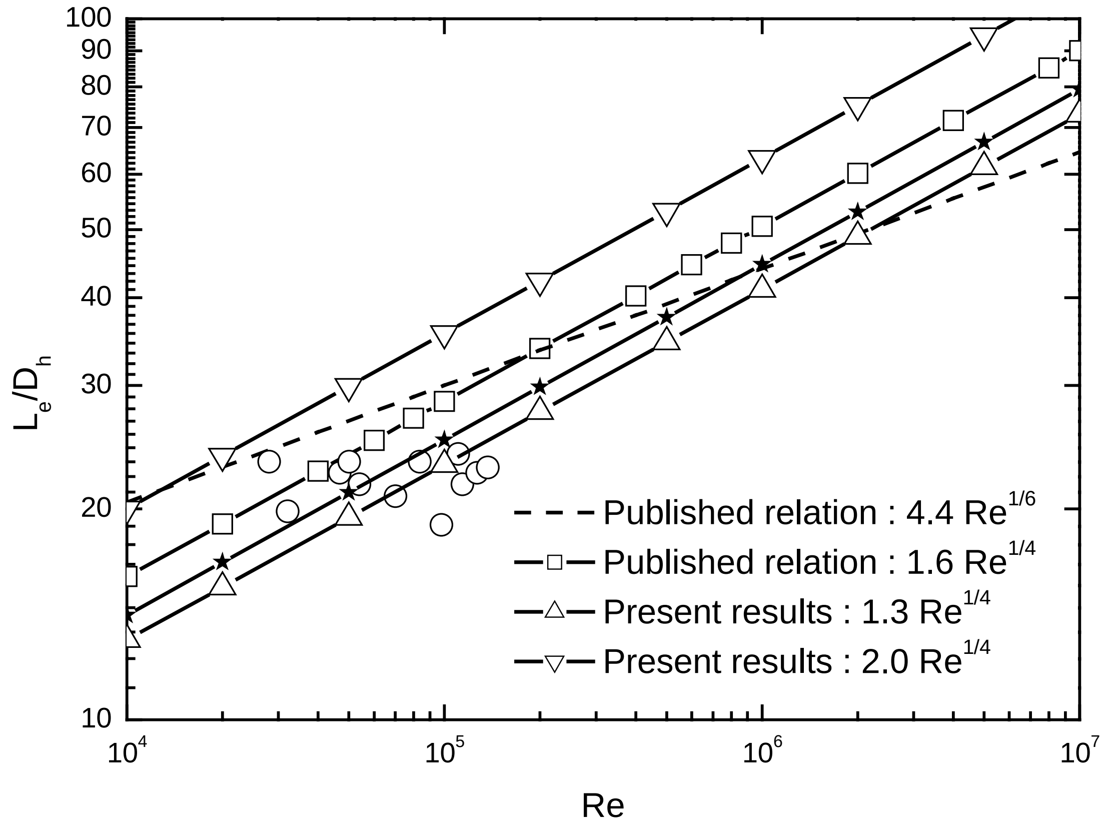

Circular pipes, D = 16 cm (■) and D = 30 cm (☆)

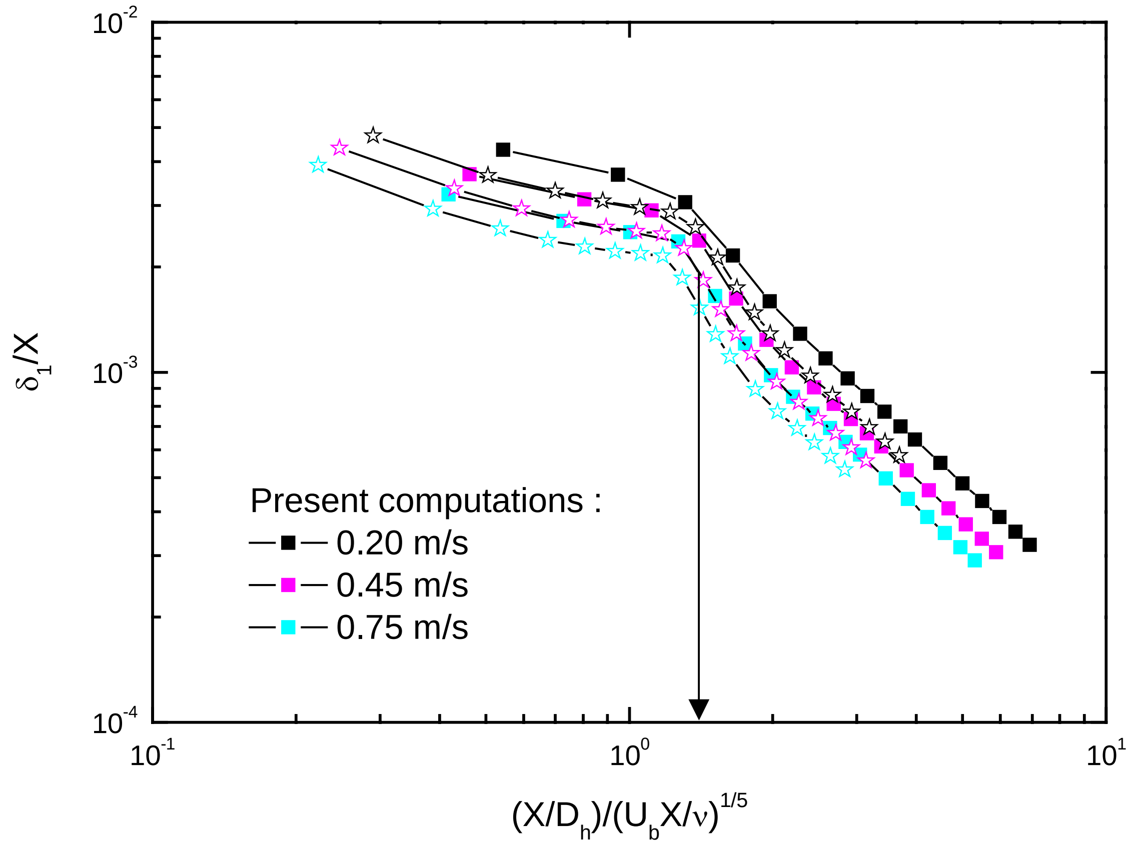

Square duct, d = 60 cm (■) and open channel h = 30 cm (☆)

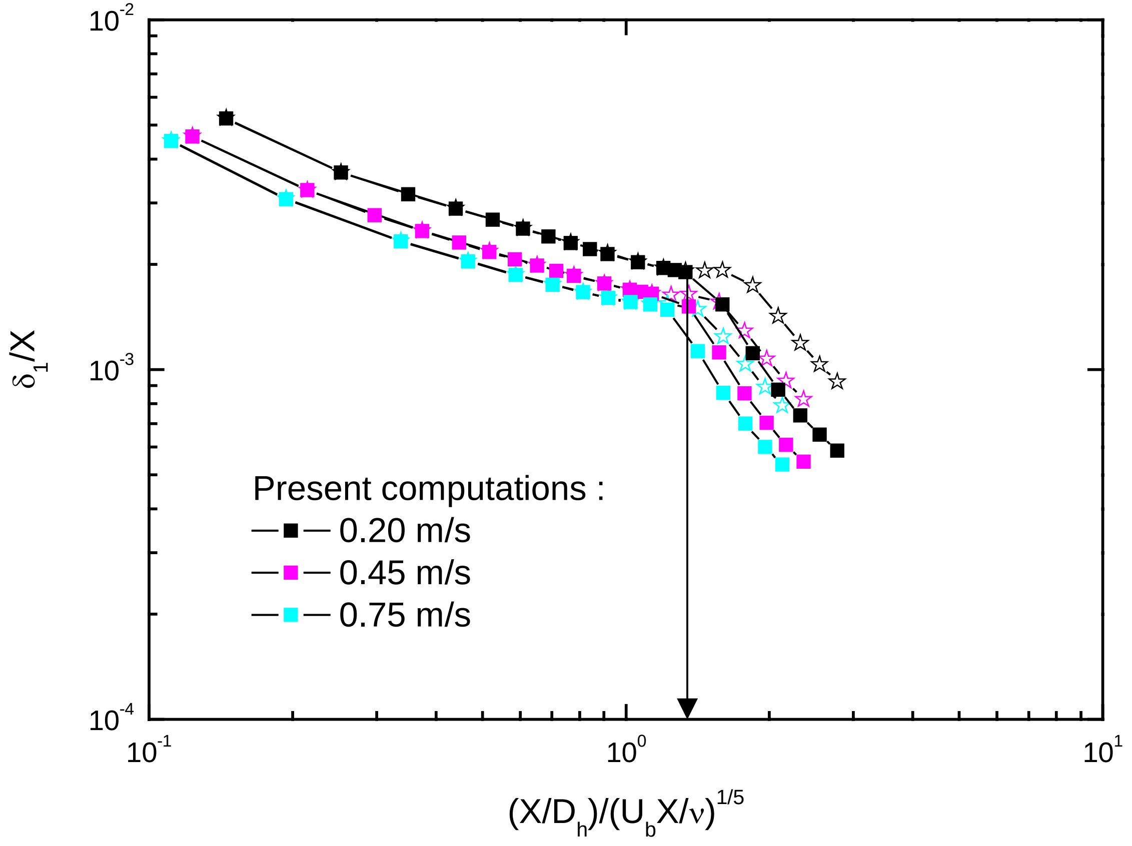

Compilation of square duct data by Demuren and Rodi (1984), ■
Open channel data measured by Nezu and Rodi (1986), ★

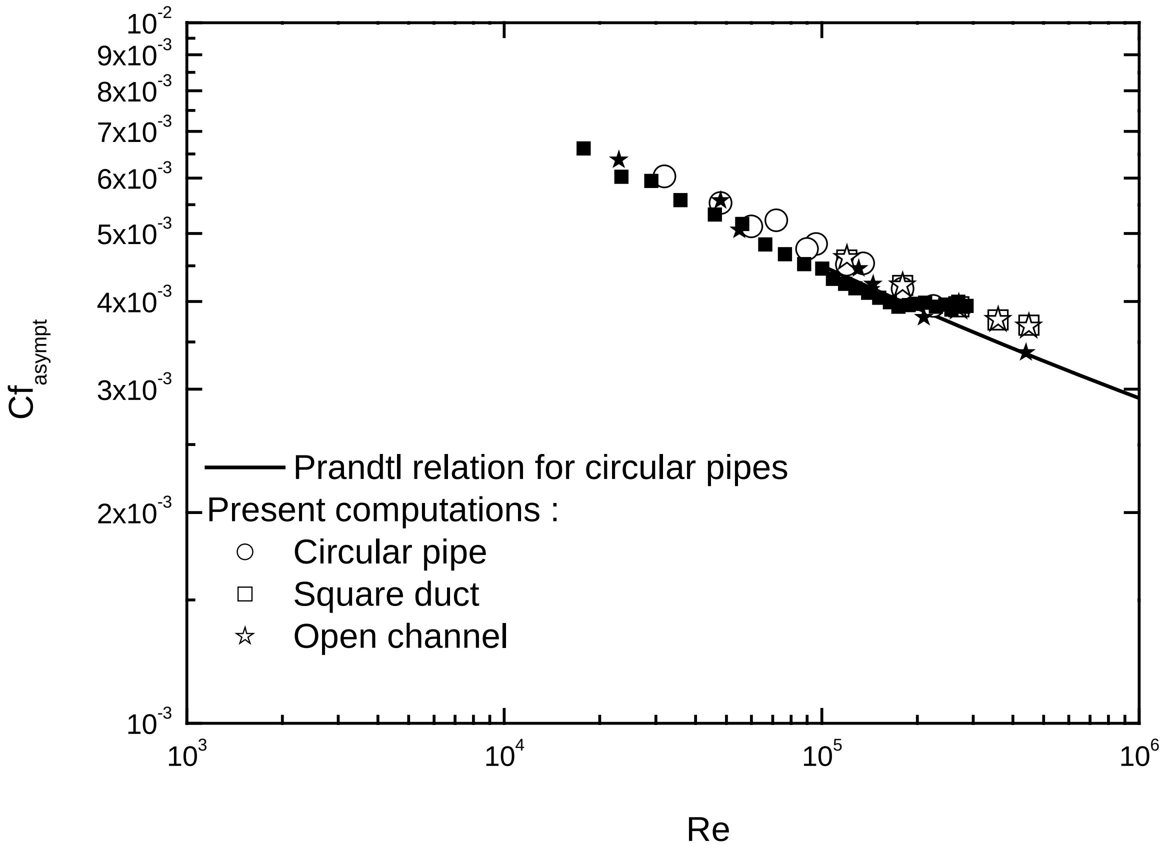

Asymptotic values in the developed region

Compilation of pipe flow data by Coantic (1966), ---○---
Compilation of plane channel data by Dean (1978), ---■---
Compilation of square duct data by Demuren and Rodi (1984), ---□---
Open channel data measured by Nezu and Rodi (1986), ---★---

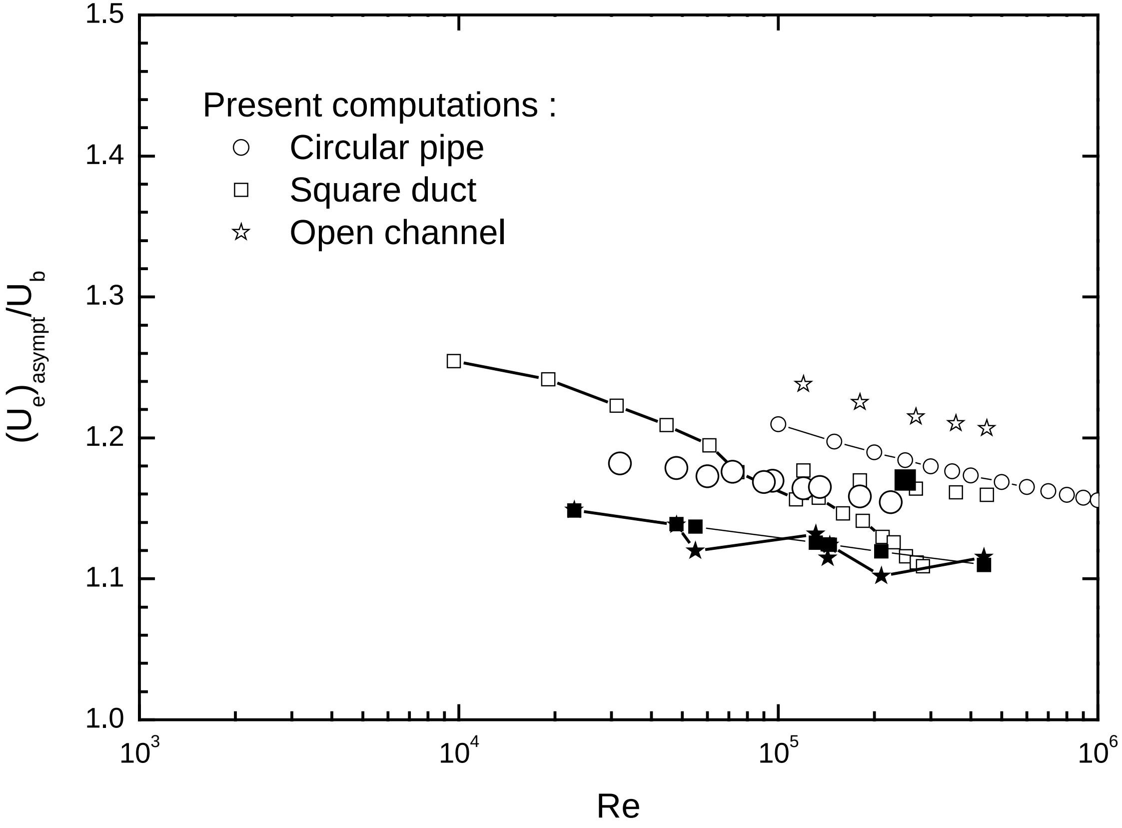

Similarities / differences with laminar conditions

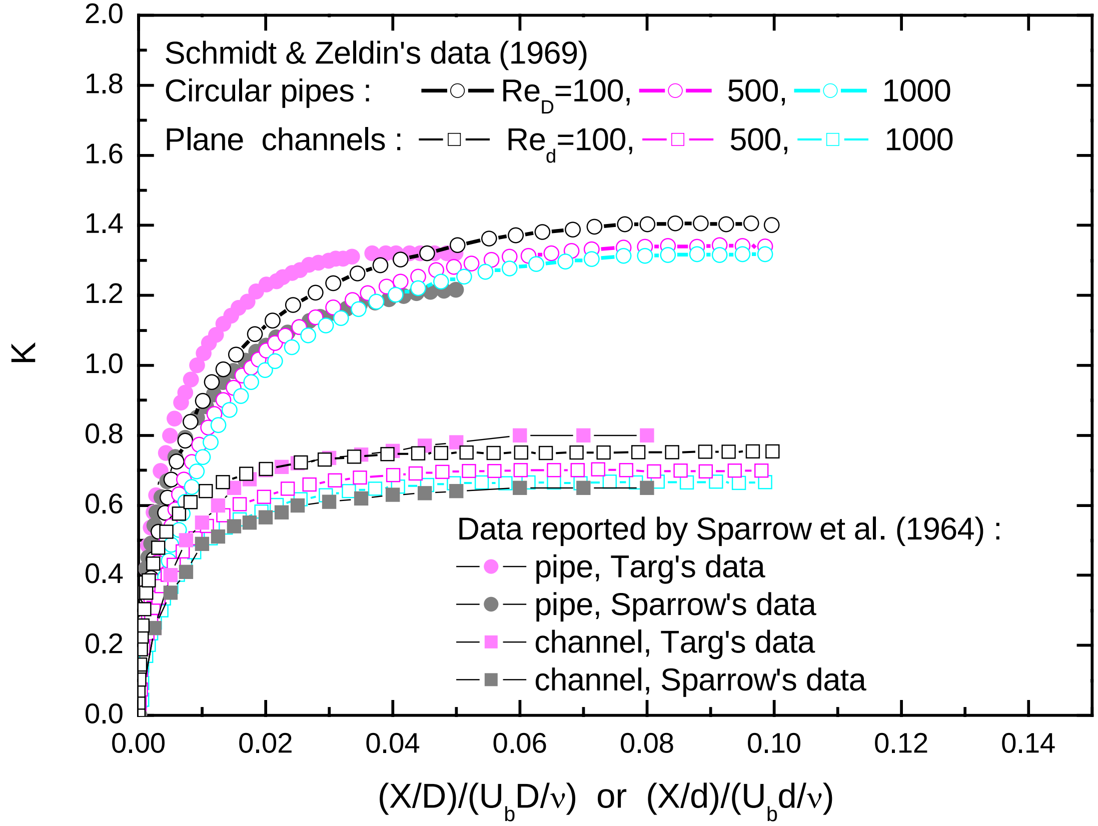

Laminar flows seem to display weaker universal behaviour : role of (specific) instabilities for pipe flows ?

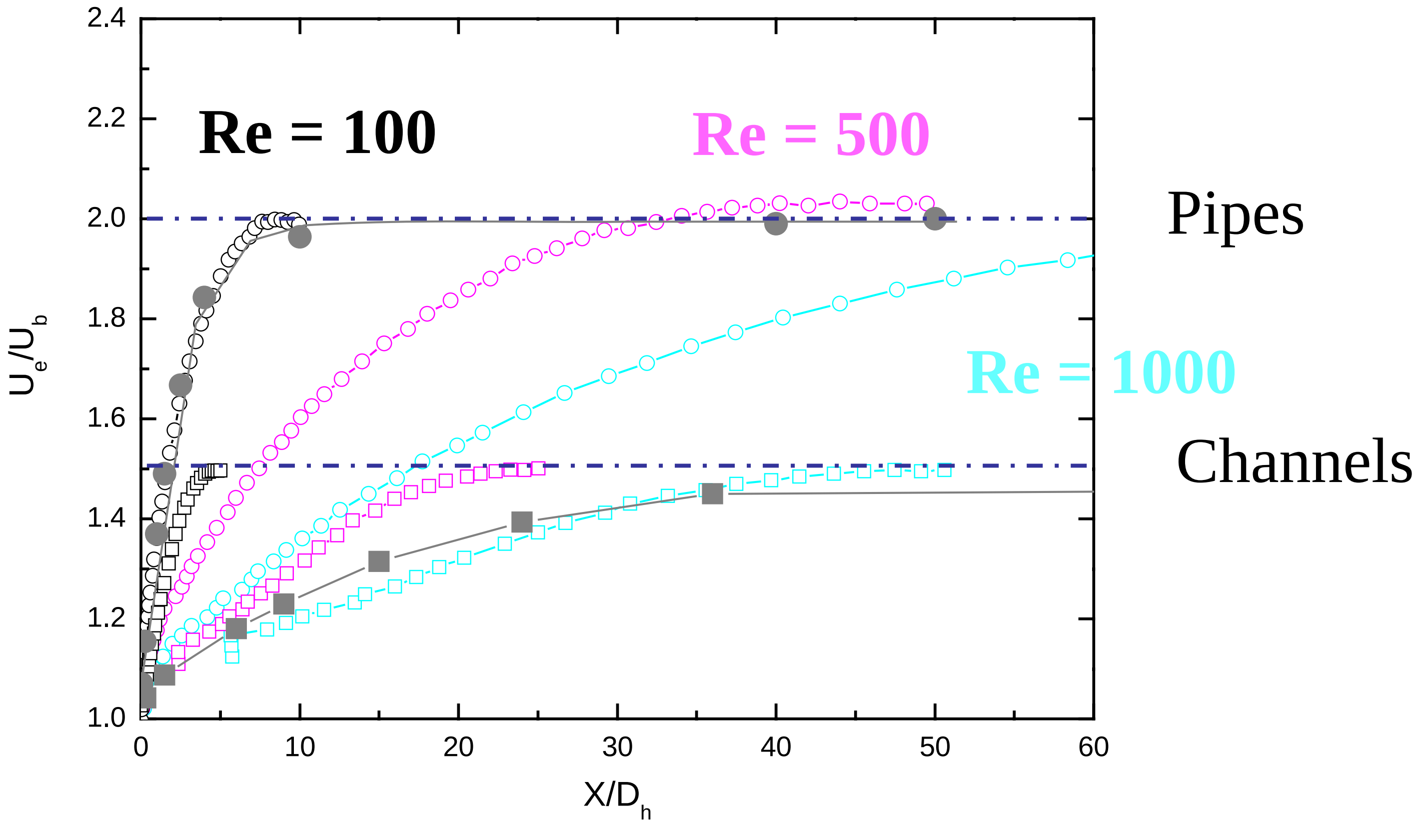
Re = 100
Re = 500
Re = 1000
Pipes
Channels
U_e/U_b
X/D_h
2.4
2.2
2.0
1.8
1.6
1.4
1.2
1.0
0
10
20
30
40
50
60

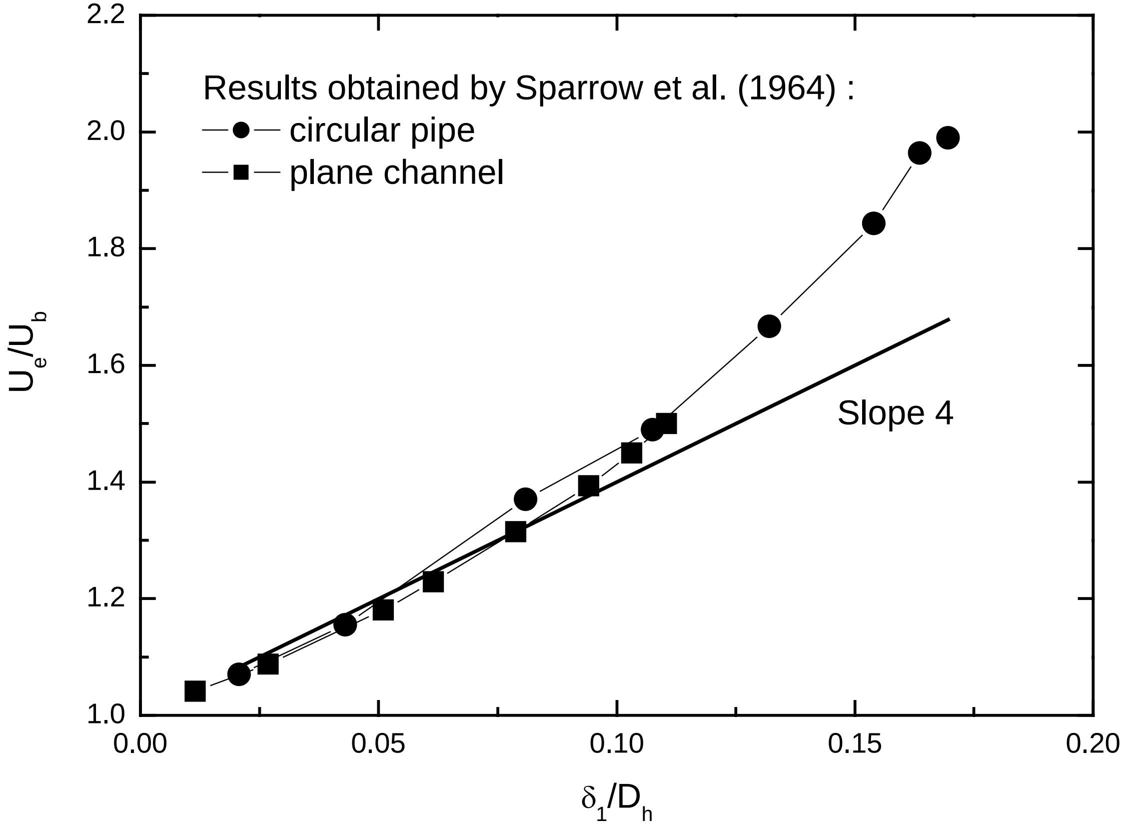
Results obtained by Sparrow et al. (1964) :
circular pipe
plane channel
Slope 4
U_e/U_b
δ_1/D_h
2.2
2.0
1.8
1.6
1.4
1.2
1.0
0.00
0.05
0.10
0.15
0.20

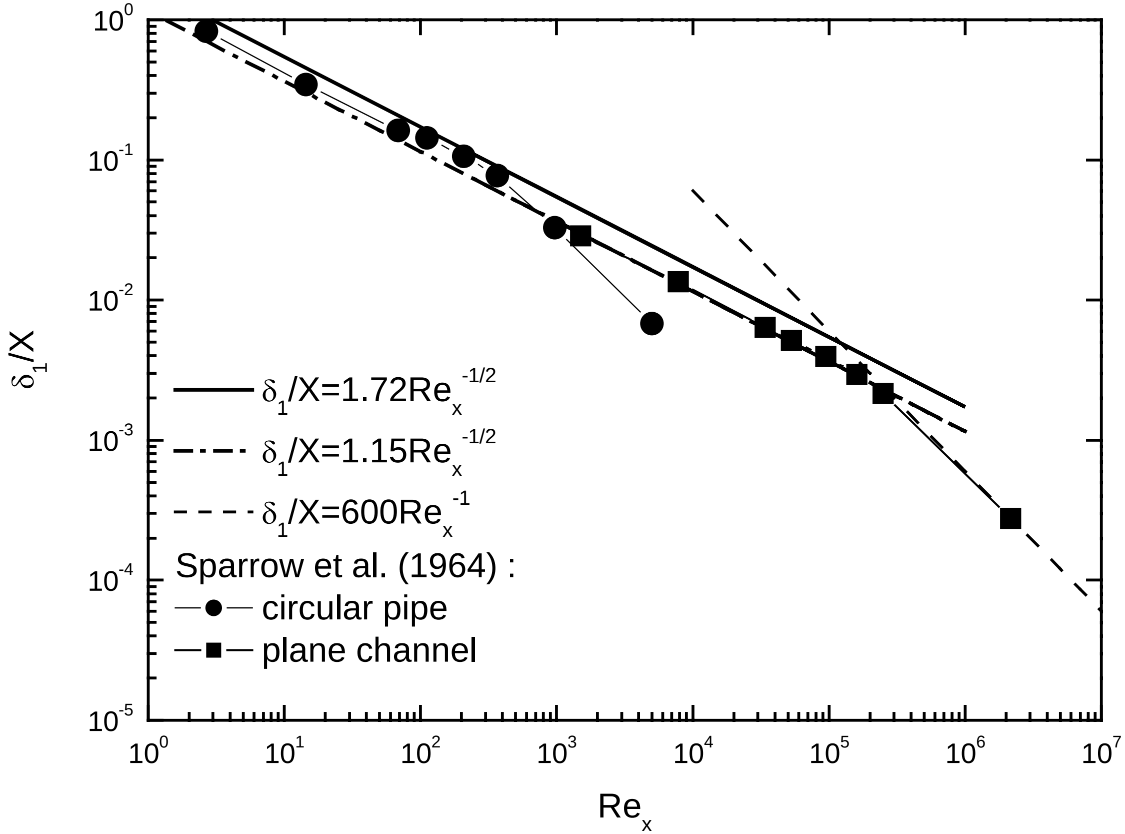

$(\delta_1)_{asympt} = \delta/3 = d/6$, Re = 600 $\Rightarrow$ $\frac{\delta_1}{X} = \frac{1}{6}\,\frac{d}{X}\,\frac{U_b/\nu}{U_e/\nu}\,\frac{U_e}{U_b} = \frac{600}{Re_X}$

Conclusion

- Acceleration in the development region of pipe, duct and open channel flows is a unique linear function of δ_1/D_h

  - Development length L_e is a function of $(Re)^{1/4}$ and not $(Re)^{1/6}$ (…… as written in most monographs)
  - Acceleration scales as $(X/D_h)/(Re)^{1/4}$ and not $(X/D_h)/(Re)$ (…… as is the case for laminar flows)

- Influence of secondary vortices in the corners is negligible for these flow features
- k-ε model is sufficiently accurate for studying such properties of the development region

We are now ready to use the water channel for studying specific problems associated with turbulent boundary layers ………

Cohesive sediment properties

(Fabien TERNAT's thesis, 2007)

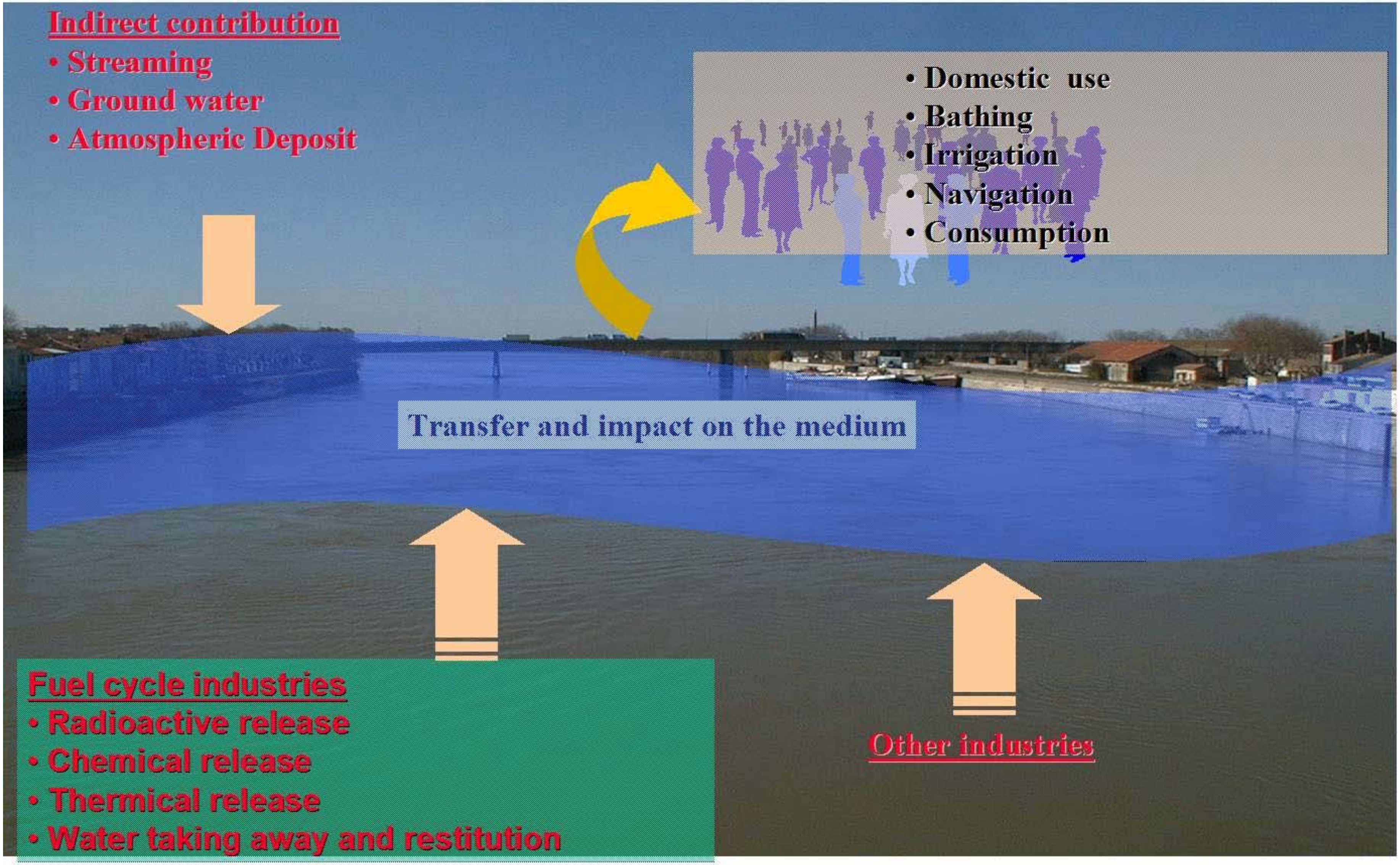

- For pollutant transport/storage in rivers (radionuclide/metallic elements), fine cohesive particles are essential because of their affinity with such positive ions.

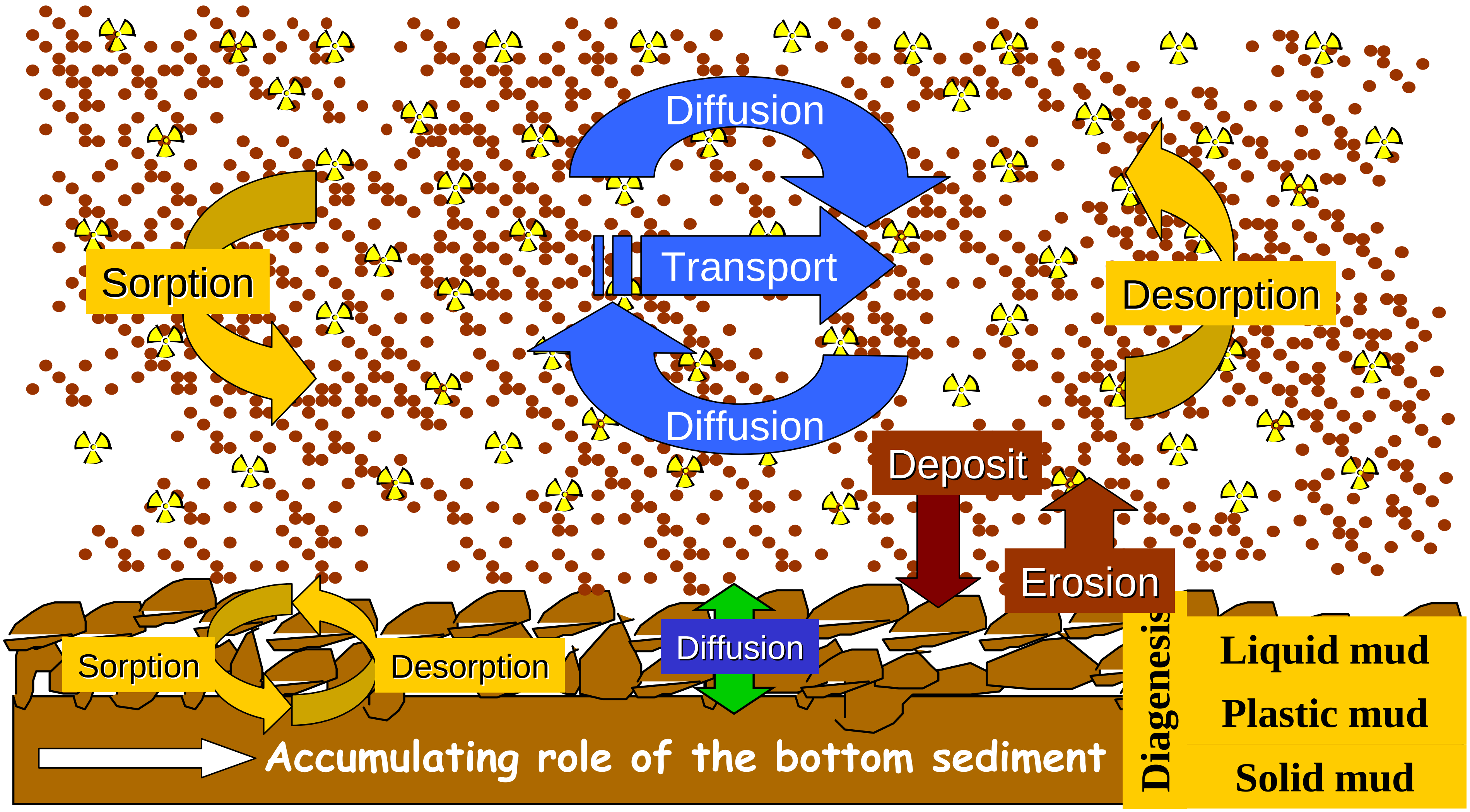
Diffusion
Sorption
Transport
Desorption
Diffusion
Deposit
Erosion
Diffusion
Sorption
Desorption
Accumulating role of the bottom sediment
Diagenesis
Liquid mud
Plastic mud
Solid mud

- Very little is known about the properties of cohesive sediment :

* erosion is modelled through threshold laws like Partheniades' (1965) :

$$\begin{cases} E = \alpha\,(\tau - \tau_{ce})^{\beta} \quad \text{if} \quad \tau > \tau_{ce}, \\ E = 0 \quad \text{if} \quad \tau < \tau_{ce} \end{cases}$$

* τ_{ce} is « much larger » for cohesive than for non-cohesive sediment,
* β is generally considered equal to 1,
* for non-cohesive sediment, Shields' diagram allows to collapse all data

Can we derive a « general » model to account for the cohesive effect ?

$$\theta \text{ (or } \tau^*) = \frac{\tau_{ce}}{(\rho_s - \rho_w)gd} = \frac{\rho_w u_{ce}^{*2}}{(\rho_s - \rho_w)gd} = \frac{\text{Wall friction}}{\text{Buoyant weight}}$$

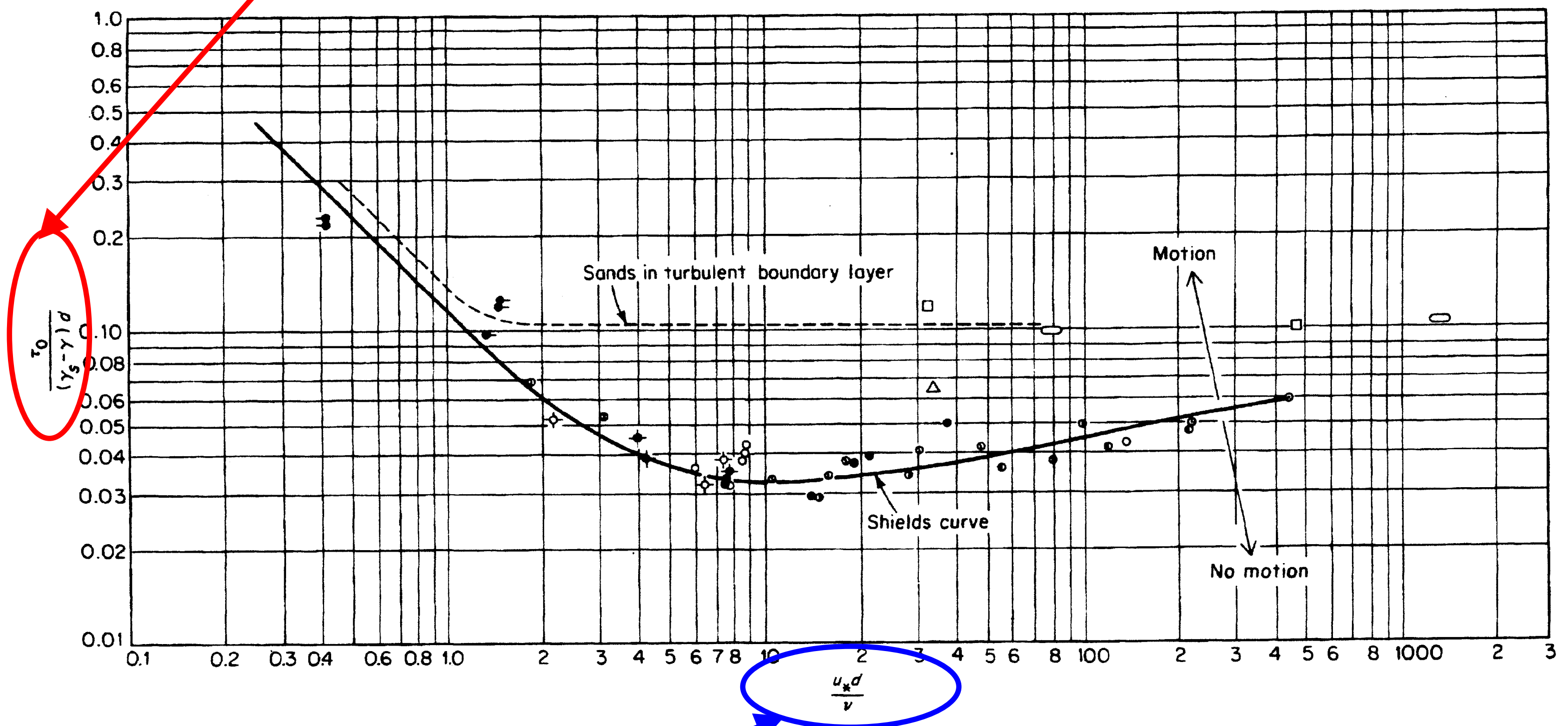

Particle Reynolds number, $Re^* = \frac{u_{ce}^* d}{\nu}$

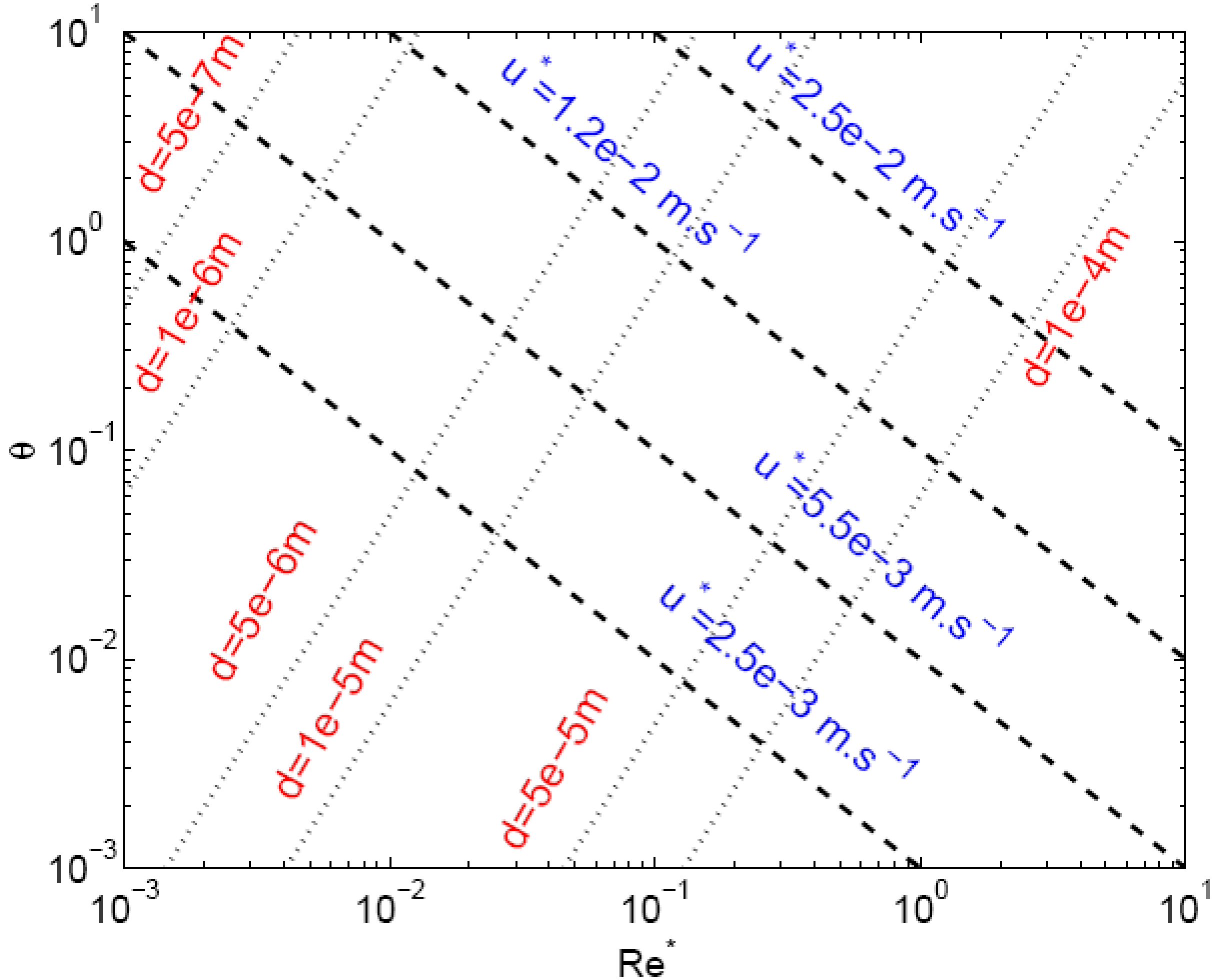

$d = \text{cste} : \theta = Re^{*2}(\rho_w \nu^2/((\rho_s - \rho_w) g d^3))$

$u^* = \text{cste} : \theta = Re^{*-1}(\rho_w u^{*3}/((\rho_s - \rho_w) g \nu))$

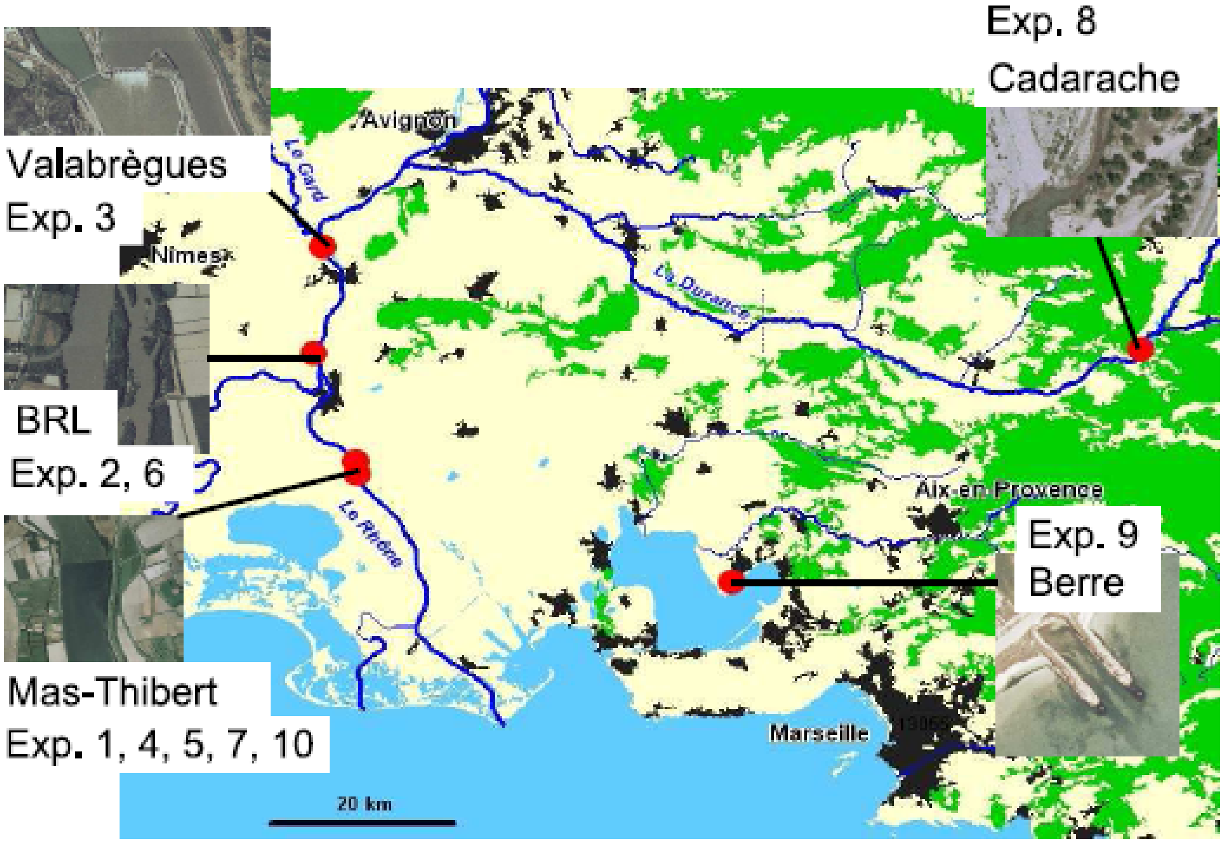

. Localisation of the different sites of core sampling for the resuspension campaigns.

1)

2)

3)

4)

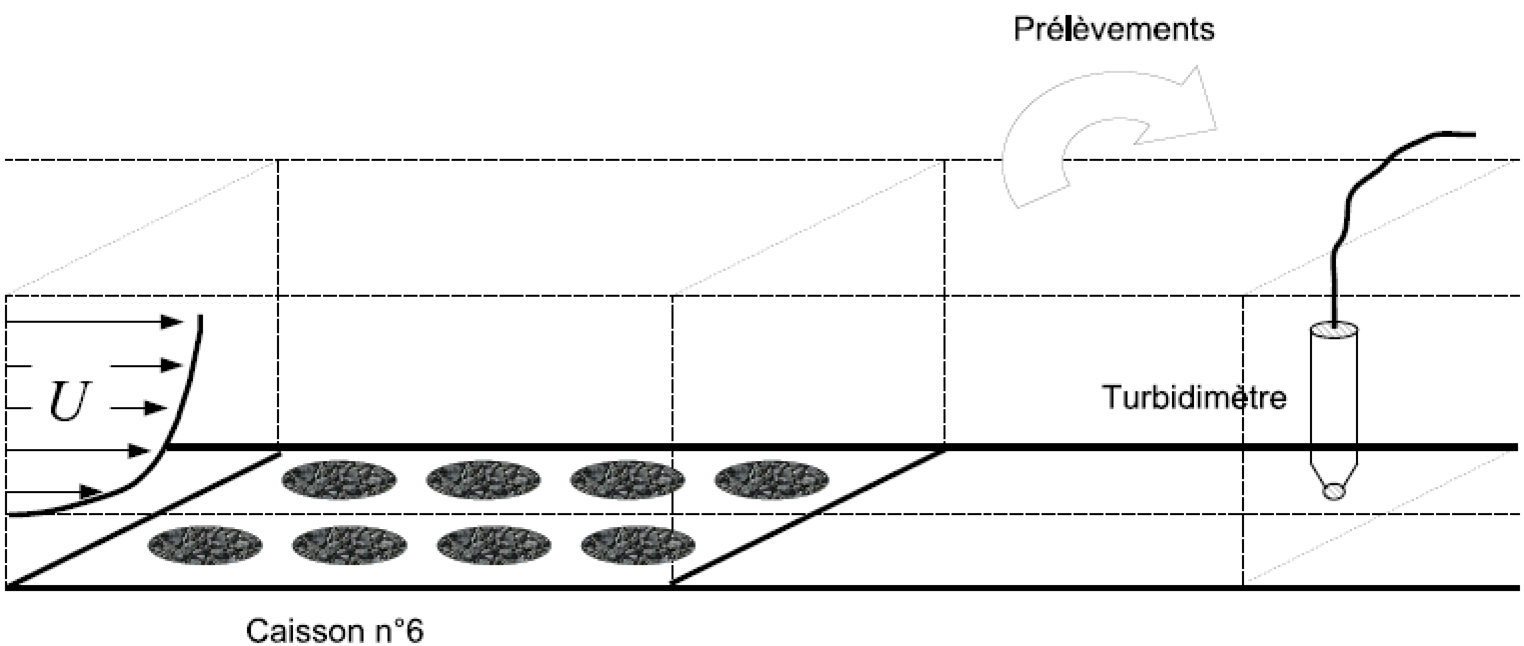
Prélèvements
U
Turbidimètre
Caisson n°6

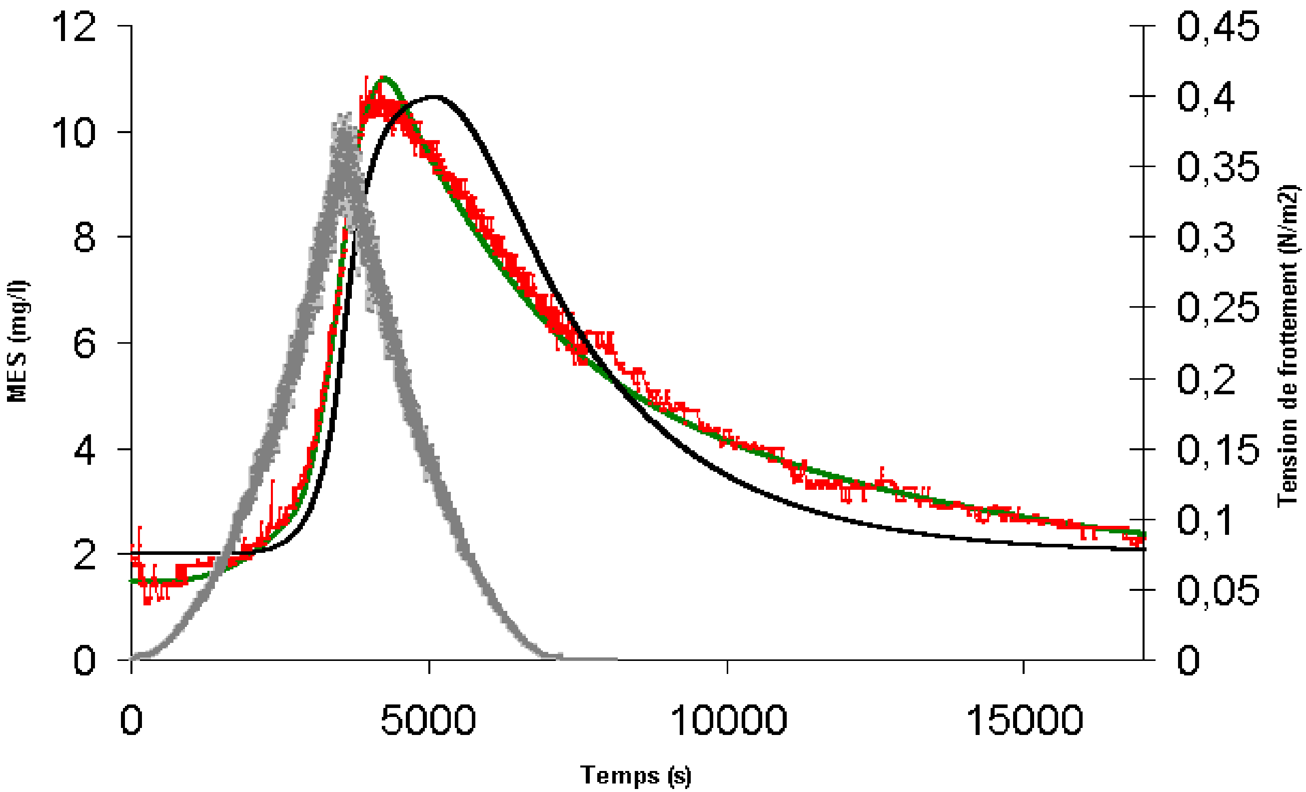

using : $$\tau_f = \frac{\rho B}{2}\left(\frac{xC}{D_h}Re_b^{-1/5}+1\right)^{9/5} U_b^2 Re_b^{-1/5}$$

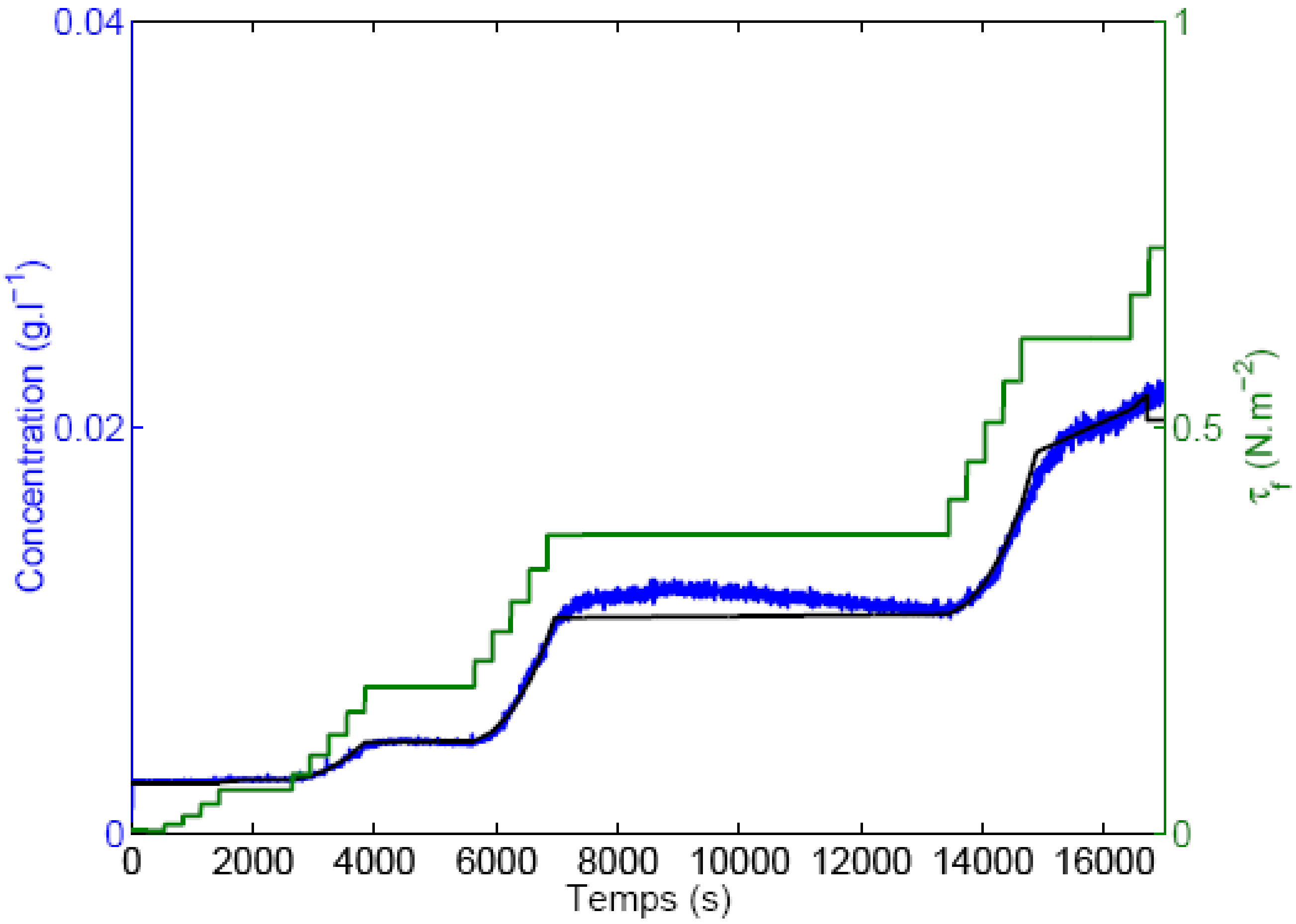

Different sediment classes associated with increasing τ_{ce} values

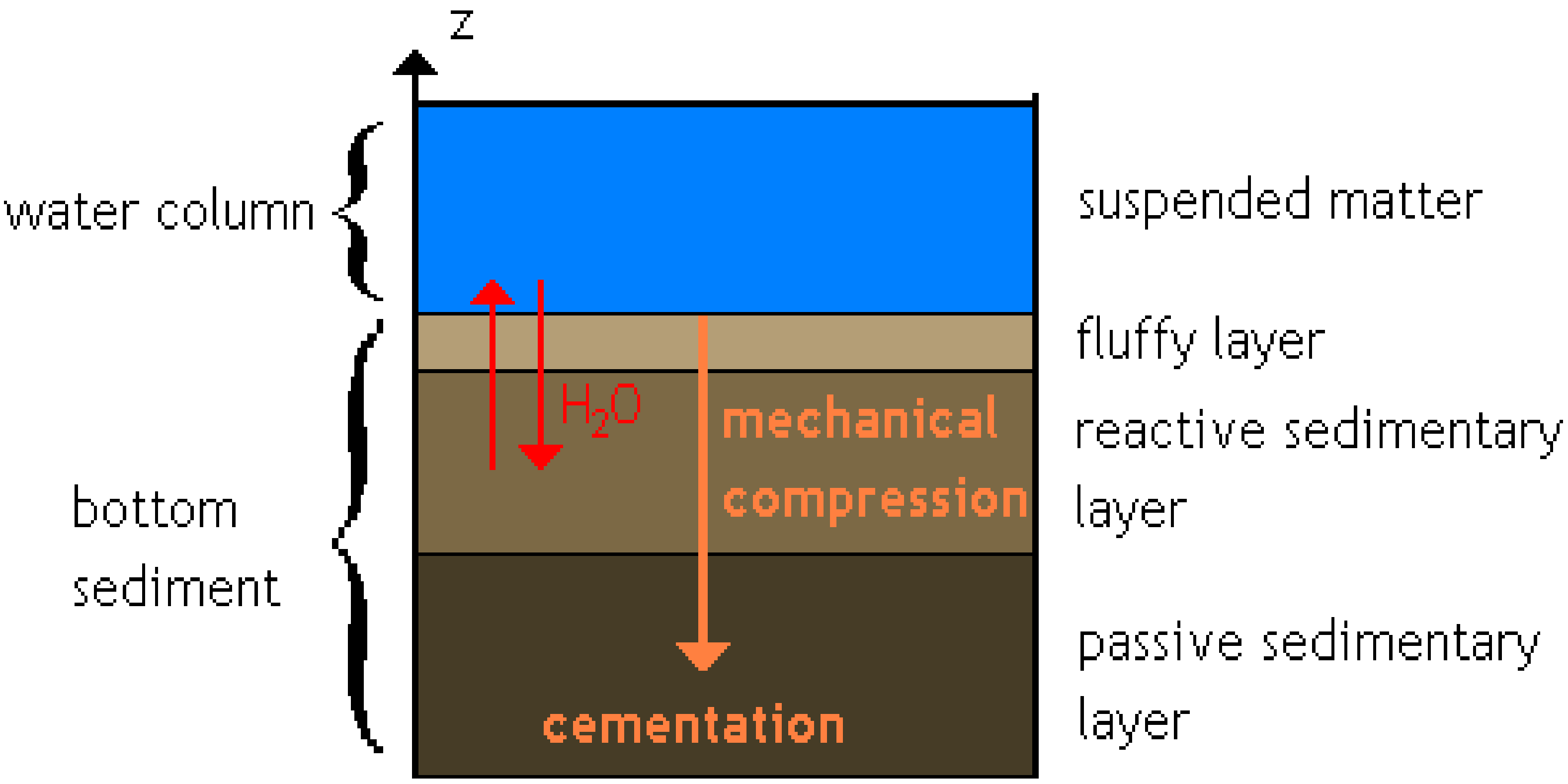
z
water column
bottom
sediment
H_2O
mechanical
compression
cementation
suspended matter
fluffy layer
reactive sedimentary
layer
passive sedimentary
layer

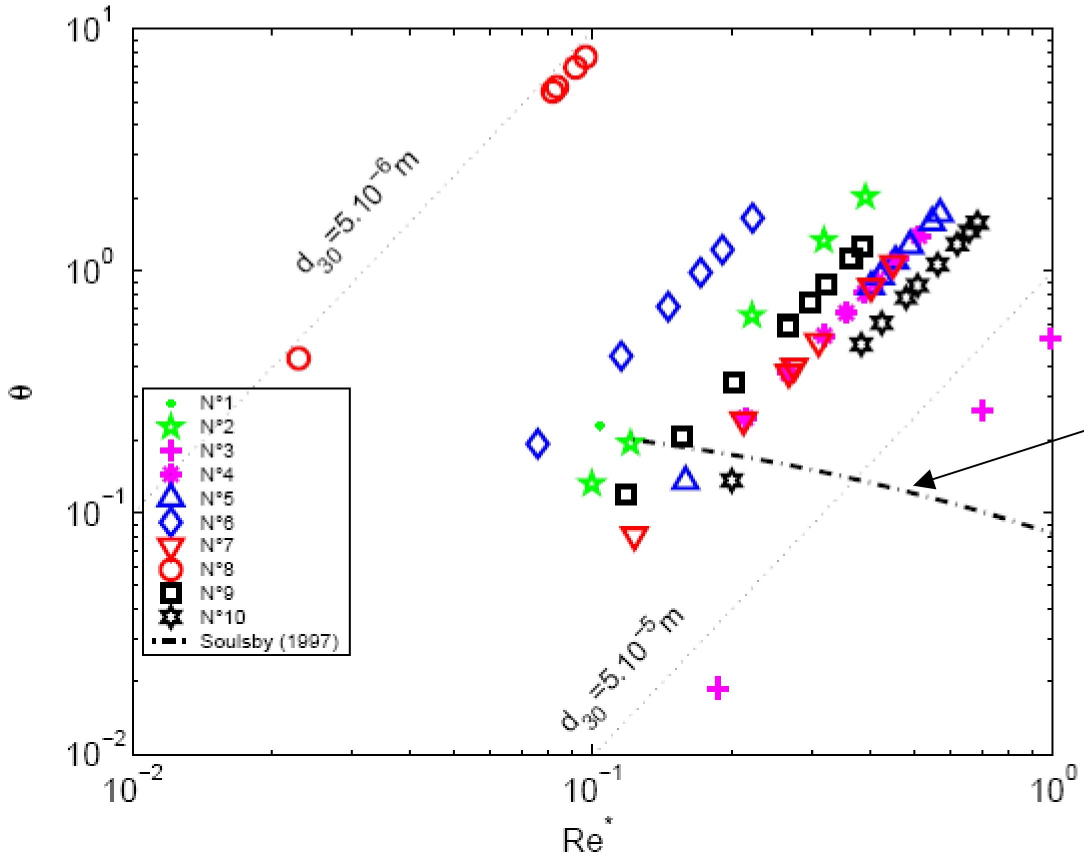

Shields/Soulsby

Experimental measurements of the erosion threshold presented in the Shields diagram for the 10 campaigns.

Our domain of interest : Re* < 1

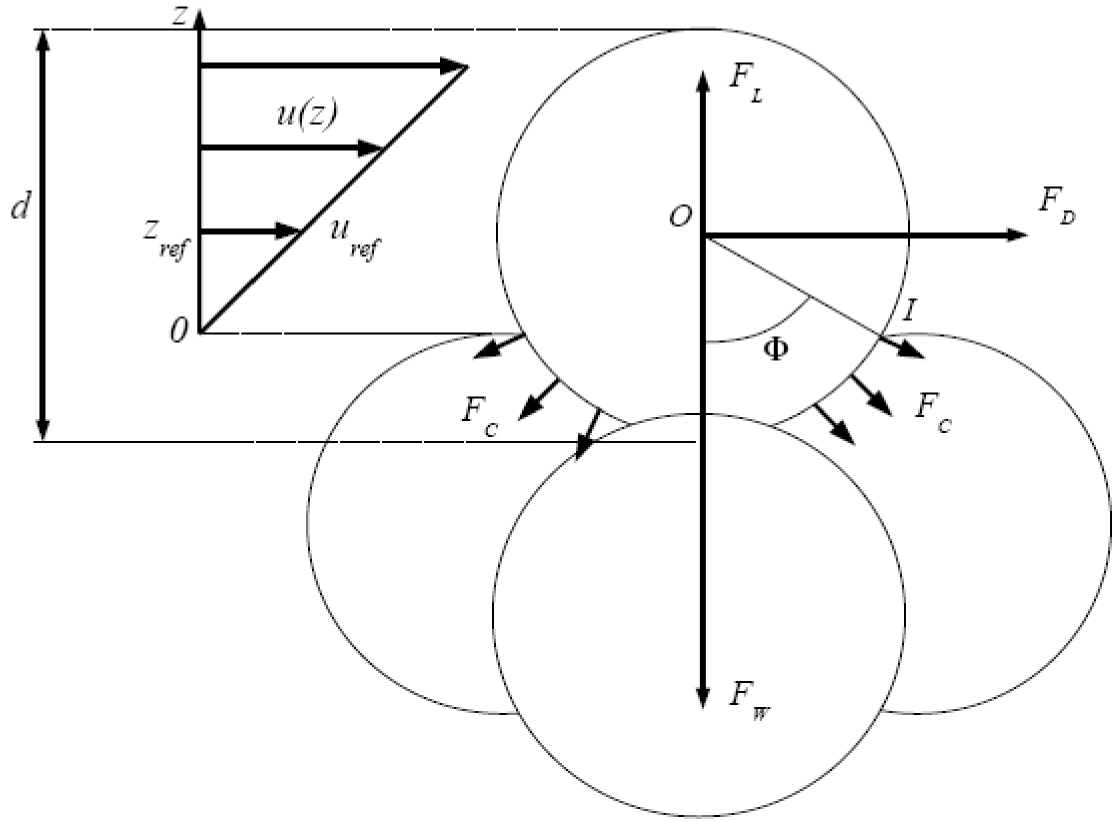

Balance between :

- the buoyant weight of the particle F_W;
- the drag force of the overlying flow F_D;
- the lift force of the overlying flow F_L;
- the cohesion force F_C.

The particle « moves » (rotation around the vertex I) if

$$\boxed{F_D = \tan\Phi \cdot (F_W - F_L + F_C)}$$

(Φ is a characteristic internal friction angle)

$$F_W = k_W.g.(\rho_s - \rho_w).d^3$$

$$\left.\begin{aligned} C_D &= \frac{24}{Re} \cdot \left(1 + \frac{3}{16}.Re\right) \\ z_{ref} &= \alpha.d \\ u^+ &= z^+ \\ u_b &= \alpha.\frac{d}{\nu_w}.u^{*2} \end{aligned}\right\} \quad \begin{aligned} Re &= \alpha.Re^{*2} \\ F_D &= k_D.a.\alpha.\rho_w.\nu_w^2 Re^{*2}\left(1 + \frac{3.\alpha}{16}.Re^{*2}\right) \end{aligned}$$

$$F_L = k_L.\alpha.\rho_w.\nu_w^2.Re^{*3}$$

Erosion threshold : $\tau^* = \dfrac{k_W \frac{\tan\Phi}{\alpha k_D}}{a + \frac{k_L}{k_D}\tan\Phi.Re^* + \frac{3.a.\alpha}{16}.Re^{*2}}\left(1 + \dfrac{F_C}{k_W.g.(\rho_s - \rho_w).d^3}\right)$

For non cohesive sediment : $$\tau^*_{\mathbf{nc}} = \frac{k_W \frac{\tan\Phi}{\alpha k_D}}{a + \frac{k_L}{k_D}\tan\Phi . Re^* + \frac{3.a.\alpha}{16}.Re^{*2}}$$

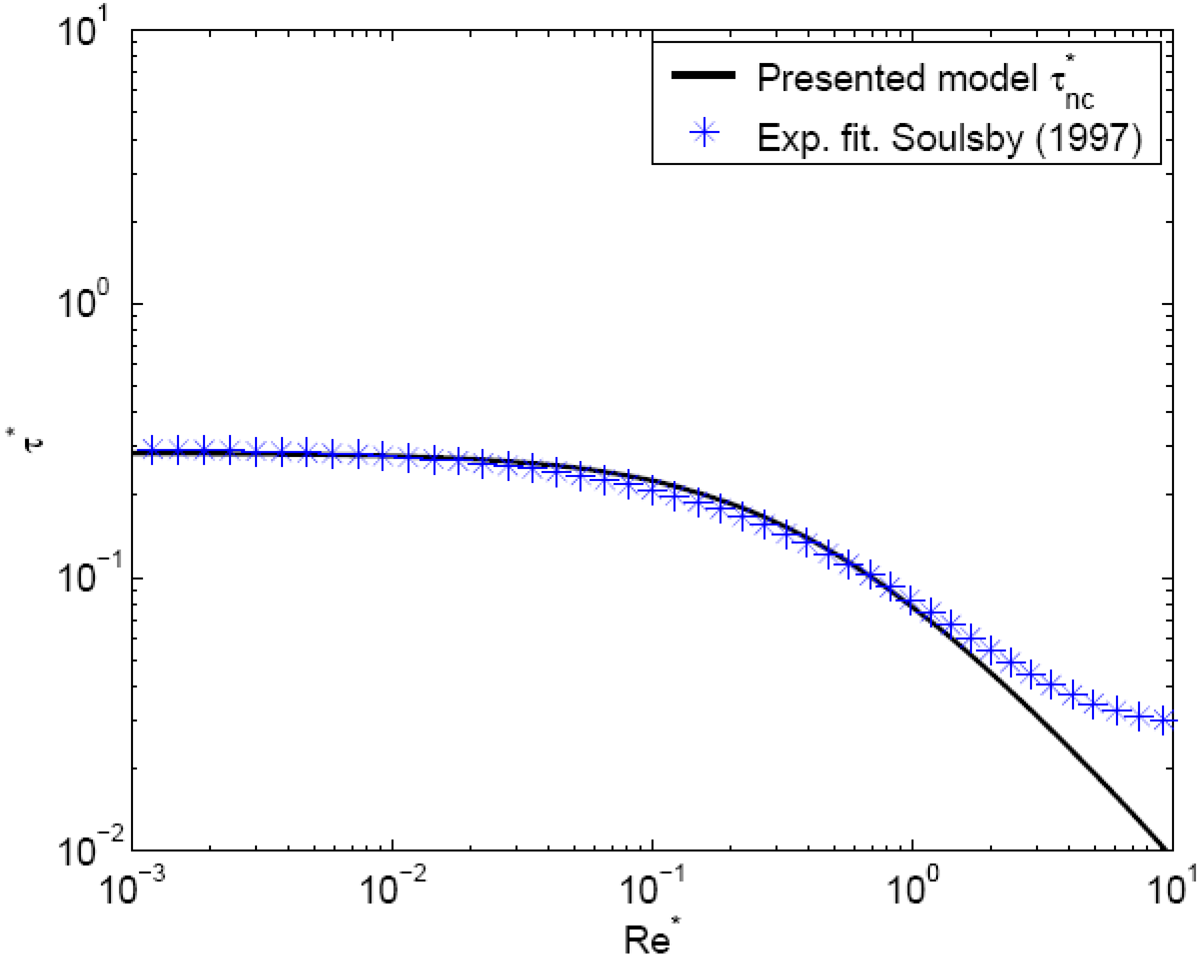

α	a	k_D	k_W	k_L	n_{max}	n_c
0, 16	37, 49	0, 4	1	30	1	0, 47

A modelling attempt of cohesion : using Van der Waals' force

For two particles :

$$F_H(n, d_1, d_2) = \frac{A_H.d_1.d_2}{12 \cdot (d_1 + d_2) \cdot d_i^2}$$

where $A_H \simeq 10^{-20} J$ is the Hamaker constant, d_1 (m) and d_2 (m) the particle diameters, d_i the interparticle distance. Typical A_H values for different argileous minerals are $2,2.10^{-20} J$ for montmorillonite and $3,1.10^{-20} J$ for kaolinite [Bergström, 1997, cited by *Gelard*, 2005]. The range of variation of d_i is given by the condition: $d_i << d_1,\ d_2$.

For any particular cristal arrangement (simple cubic, centered cubic, …), the compaction factor is defined (as the ratio between the effective volume of particles and the total cristal volume) by :

$$c = \frac{\pi}{6} \cdot \left(\frac{d}{b}\right)^3 ,$$

with $b = d + d_i$, the distance between two particle centers.

Thus :

$$d_i = \left(\left(\frac{6.c}{\pi}\right)^{-1/3} - 1\right) \cdot d ,$$

with $d_i > 0$ implying that $c < c_c$ (generally equal to $\pi/6$).

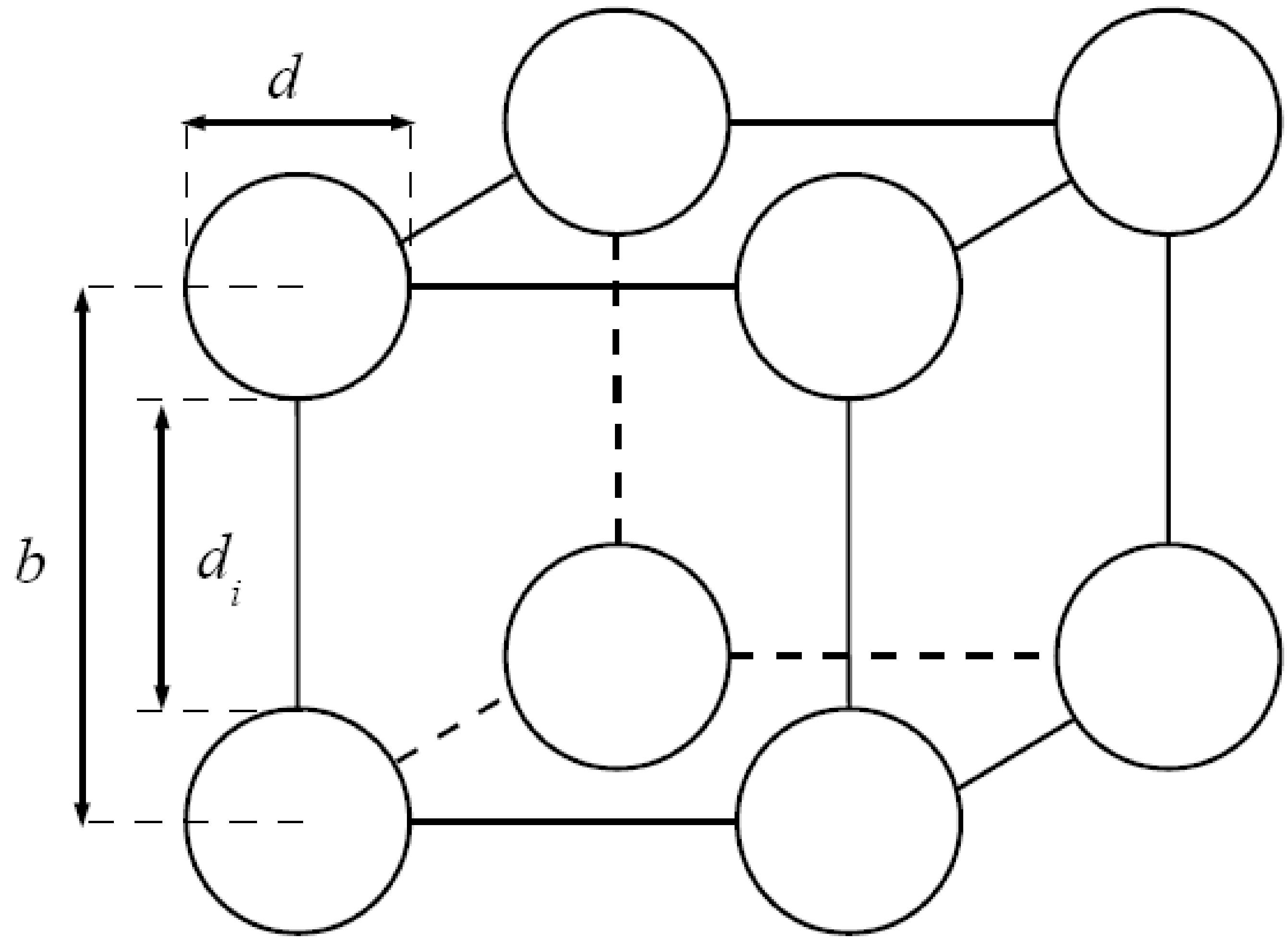
d
b
d
i

And, using the porosity n : (n = V_w/V_{tot})

$$c = \frac{n_{\max} - n}{n_{\max} - n_{\min}} \cdot c_c$$

so that finally the used expression for d_i is:

$$d_i = K(n) \cdot d$$

with $K(n)$, the compaction function defined by:

$$K(n) = \left(\left(\frac{n_{\max} - n_{\min}}{n_{\max} - n} \right)^{1/3} - 1 \right)$$

If we now consider that the « small » and « big » particles are arranged like:

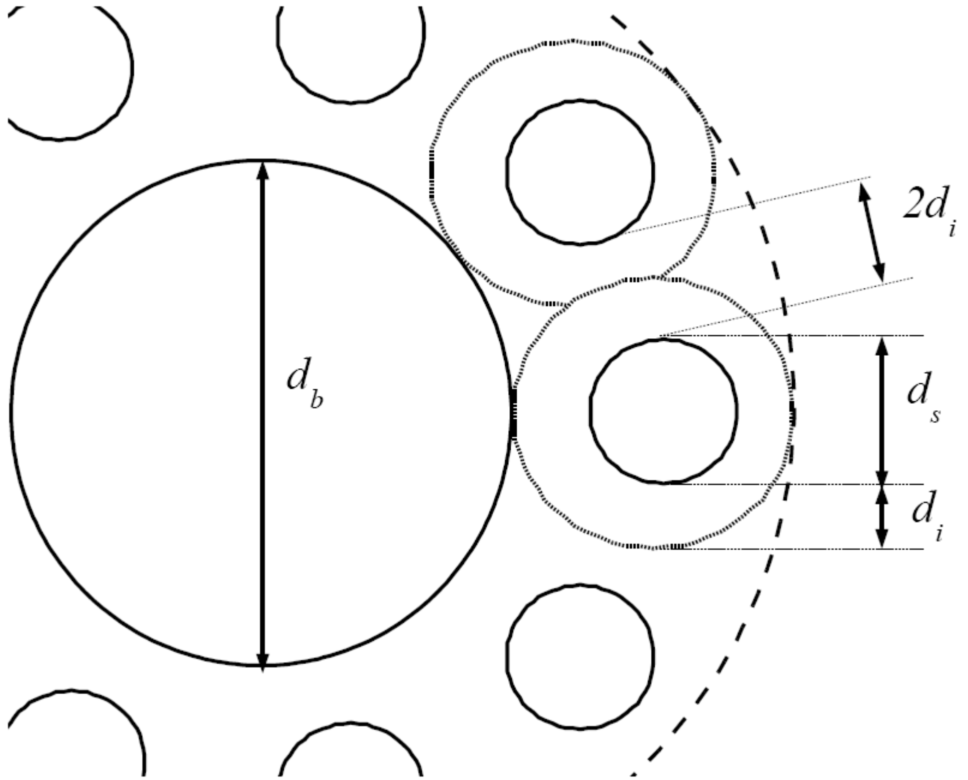

Then,

the coordination number corresponds to the number of small particles of radius $\frac{d_s}{2} + d_i$ that can be included inside the volume comprised between the big sphere and the one of radius $\frac{d_b}{2} + 2.d_i + d_s$:

$$C = \frac{V_v}{V_s}$$

with

$$V_v = \frac{4}{3} \cdot \pi \cdot \left[\left(\frac{d_b}{2} + d_s + 2.d_i \right)^3 - \left(\frac{d_b}{2} \right)^3 \right]$$

$$V_s = \frac{4}{3}\pi \cdot \left(\frac{d_s}{2} + d_i \right)^3$$

so that

$$\boxed{C = \left(\frac{d_b}{(1+2.K)d_s} \right)^3 \left[\left(1 + 2.(1+2.K)\frac{d_s}{d_b} \right)^3 - 1 \right]}$$

(with $d_i = K\ d_s$).

If we also consider that the particle is only partially buried at the Interface water/sediment:

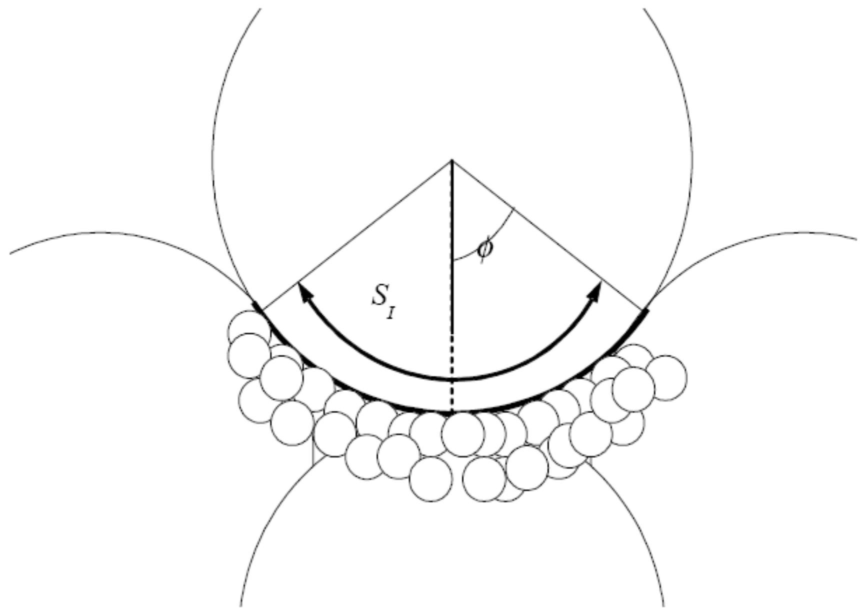

then the actual contact surface is: $$S_I = \frac{\pi \cdot d^2}{2}(1 - \cos\Phi)$$

so that C is given by:
(for any d_b/d_s pair)

$$\boxed{\begin{aligned} C_I(n, d_b, d_s) &= \left(\tfrac{1-\cos\Phi}{2}\right)\left(\tfrac{d_b}{(1+2.K(n))d_s}\right)^3 \\ &\left[\left(1+2.(1+2.K(n))\tfrac{d_s}{d_b}\right)^3 - 1\right] \end{aligned}}$$

For a given size of « big » particles d_b, the elementary cohesion force exerted by all smaller particles of size d_s is then :

$$F_{2C}(n, d_b, d_s) = C_I(n, d_b, d_s).F_H(n, d_b, d_s).s(d_s)$$

(where s(d) is the granulometric spectrum). Then, the total cohesion force writes:

$$\begin{aligned} F_C(n, d_b) &= \int_0^\infty F_{2C}(n, d_b, d_s).dd_s \\ &= \int_0^\infty C_I(n, d_b, d_s).F_H(n, d_b, d_s).s(d_s).dd_s \end{aligned}$$

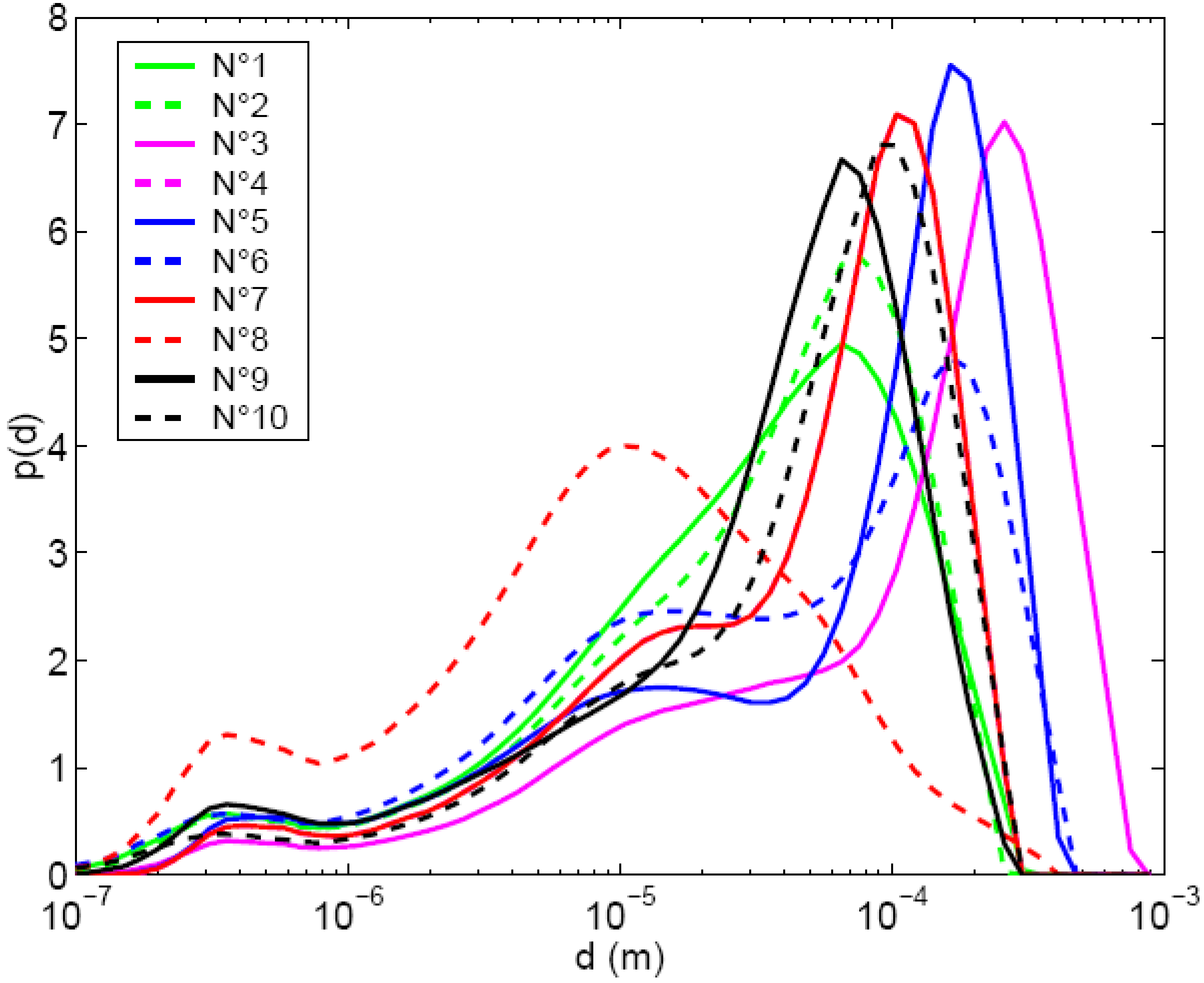

Granulometric distributions for our experiments.

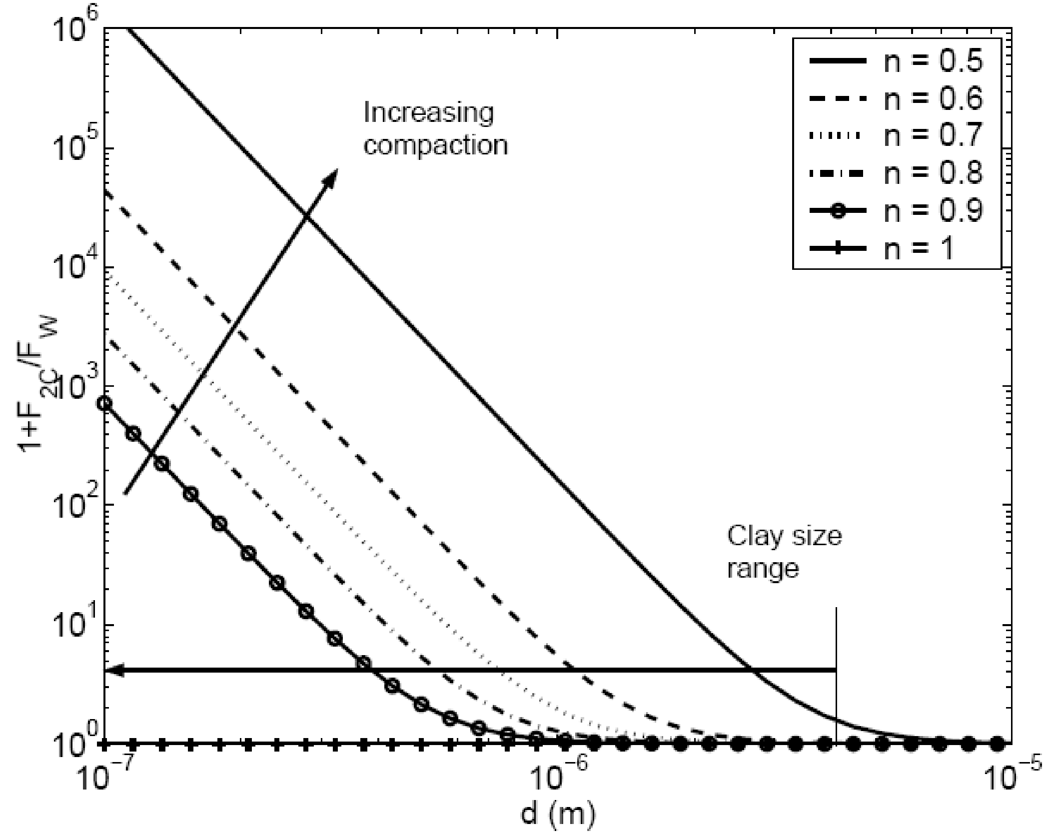

Two by two cohesion function $1+\frac{F_C}{F_W}$ vs. particle diameter d for different values of the porosity n.

ρ_s $(kg.m^{-3})$	ρ_w $(kg.m^{-3})$	g $(m.s^{-2})$	A_H (J)
2650	1000	10	1.10^{-20}
n_{max}	n_c	Φ	
(-)	(-)	(deg)	
1	$1-\frac{\pi}{6}\simeq 0.48$	$52,5$	

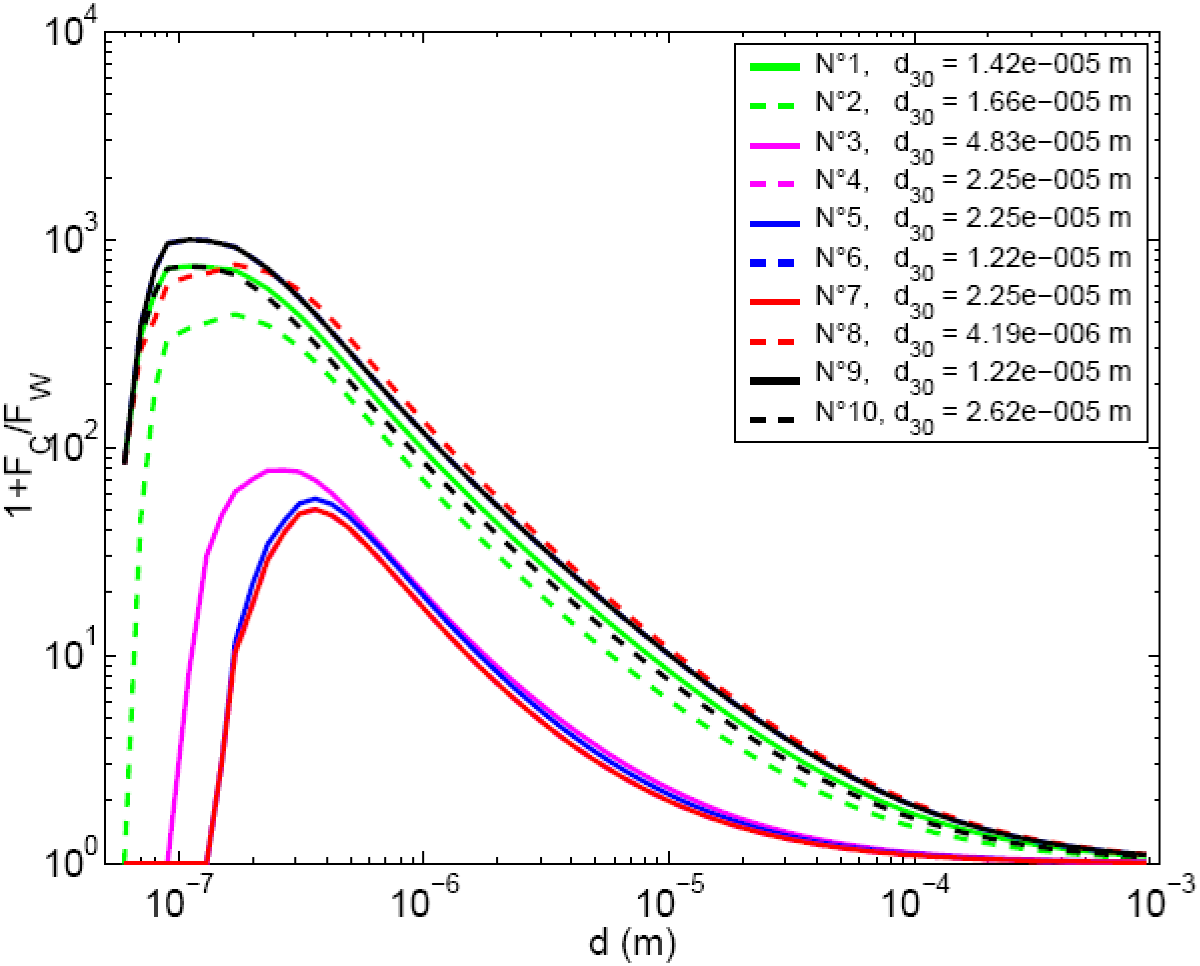

Evolution of the cohesion function $1 + \frac{F_C}{F_W}$ vs. particle diameter d for different granulometric spectra, for the same compaction degree.

Finally, the global cohesion function acting within a sediment sample is:

$$\boxed{\left\langle 1 + \frac{F_C}{F_W} \right\rangle (n) = \int_0^\infty 1 + \frac{F_C(n,d)}{F_W} s(d).dd}$$

So that u^*_{ce} is finally obtained by fiding the zeros of the relation:

$$\begin{aligned} f(d, u^*_{ce}, n) \;\; = \;\; & \frac{3.\alpha^2.k_D.a.\rho_w}{16.\nu_w^2.\tan\Phi}.d^4.u^{*4} + \frac{\alpha.k_L.\rho_w}{\nu_w} d^3.u^{*3} \\ & + \frac{\alpha.k_D.a.\rho_w}{\tan\Phi}.d^2.u^{*2} - k_W.g.\left(\rho_s - \rho_w\right).d^3 \\ & - F_C(d,n) \end{aligned}$$

(which is found to have only one positive real solution).

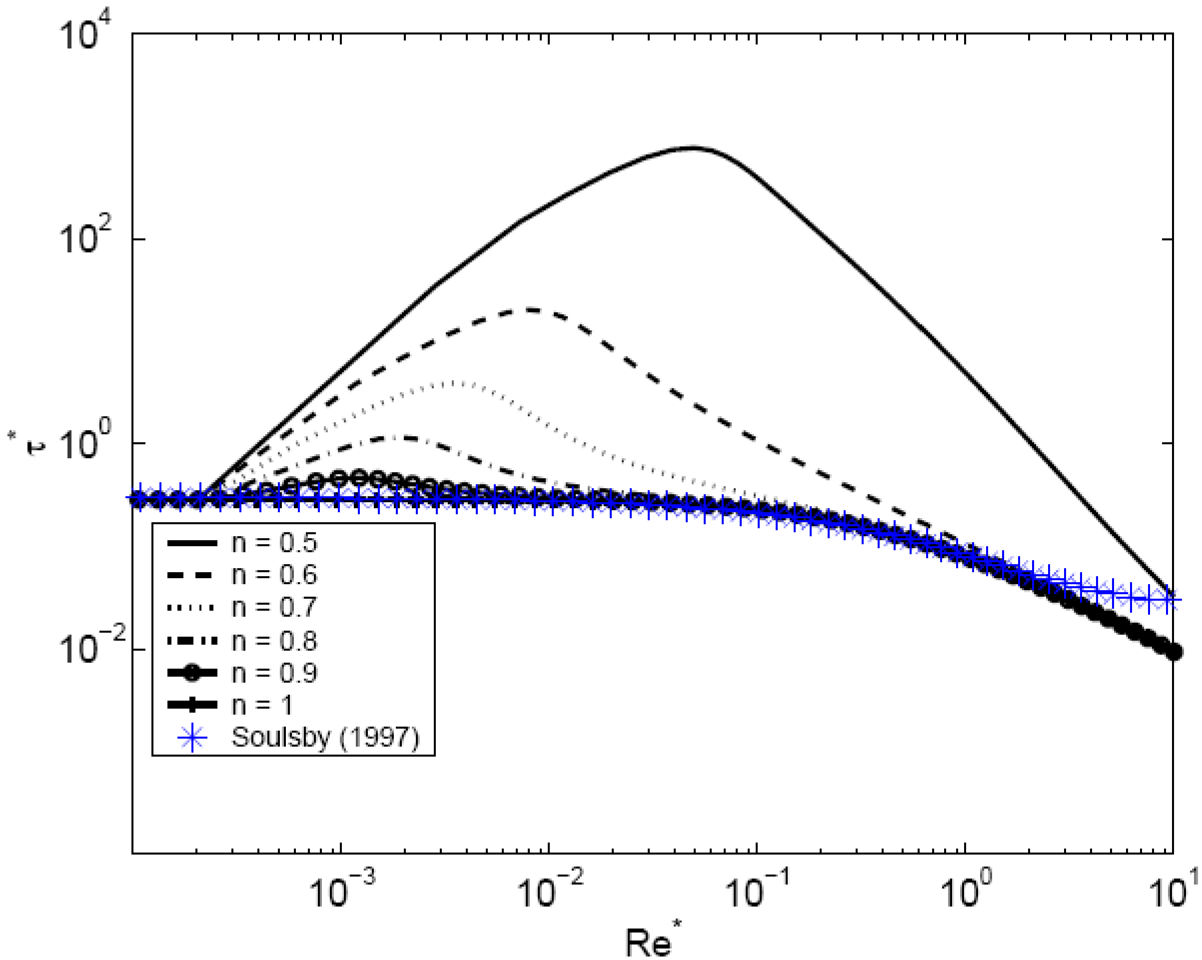

Evolution of the Shields parameter τ^* vs. the particle Reynolds number Re^* for different values of the porosity.

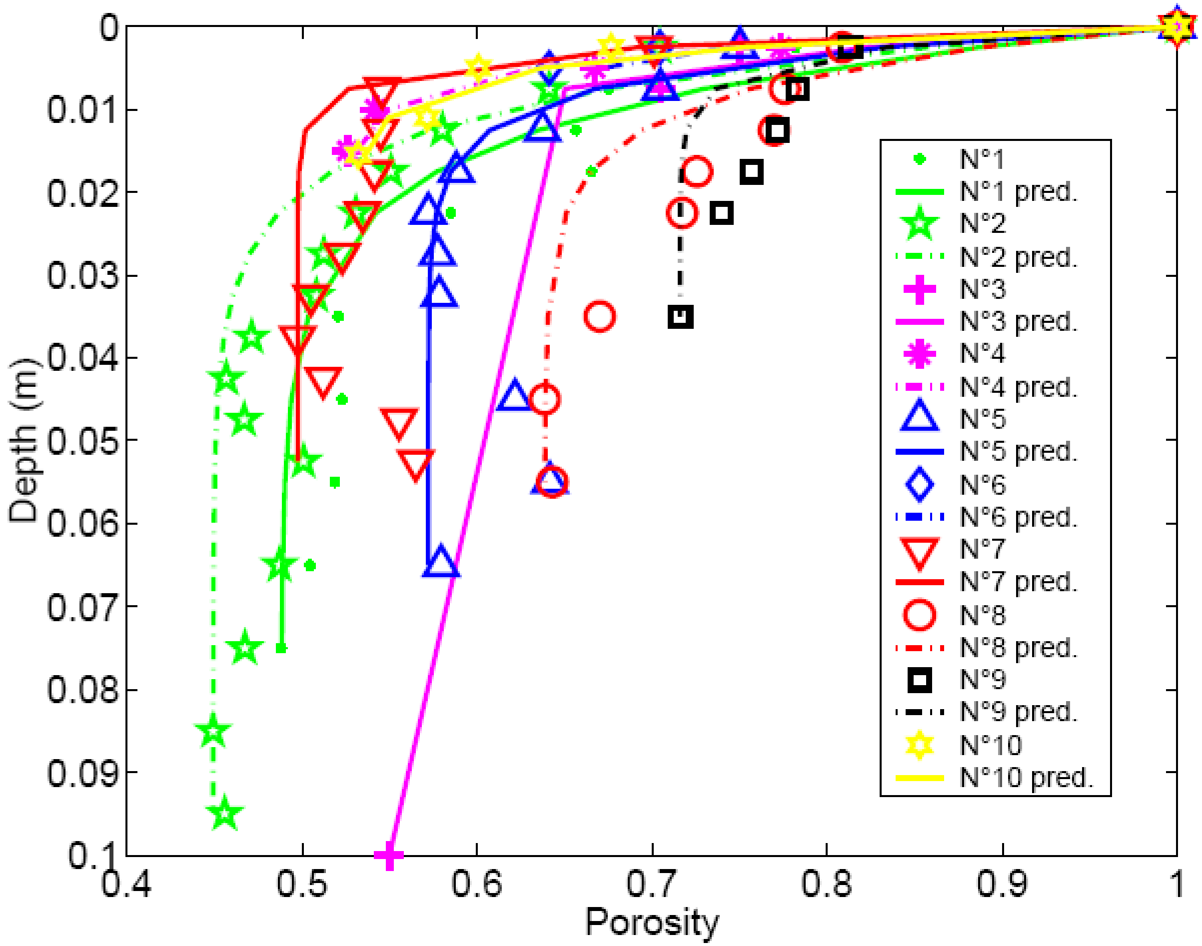

Experimental evolution of the porosity vs. depth for the 10 campaigns.

These porosity profiles are fitted according to Athy's law:

$$n(z) = n_\infty + (n_0 - n_\infty).e^{-\varsigma_s . z}$$

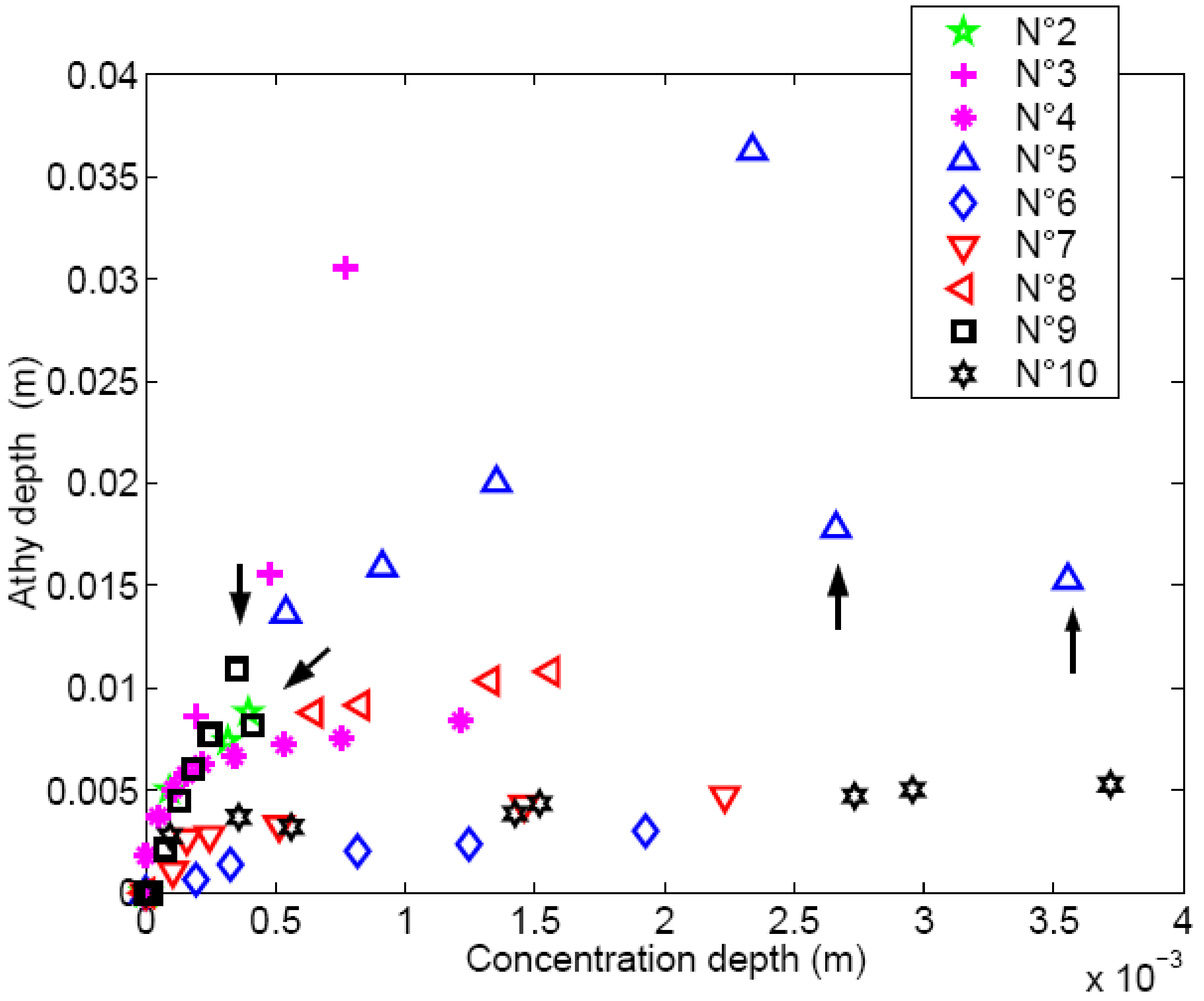

Evolution of the depth deduced from Athy's law in function of the depth deduced from concentration measurements.

The eroded depth estimated from the suspended matter concentration in the water channel has to be corrected (on the basis of Athy's law).

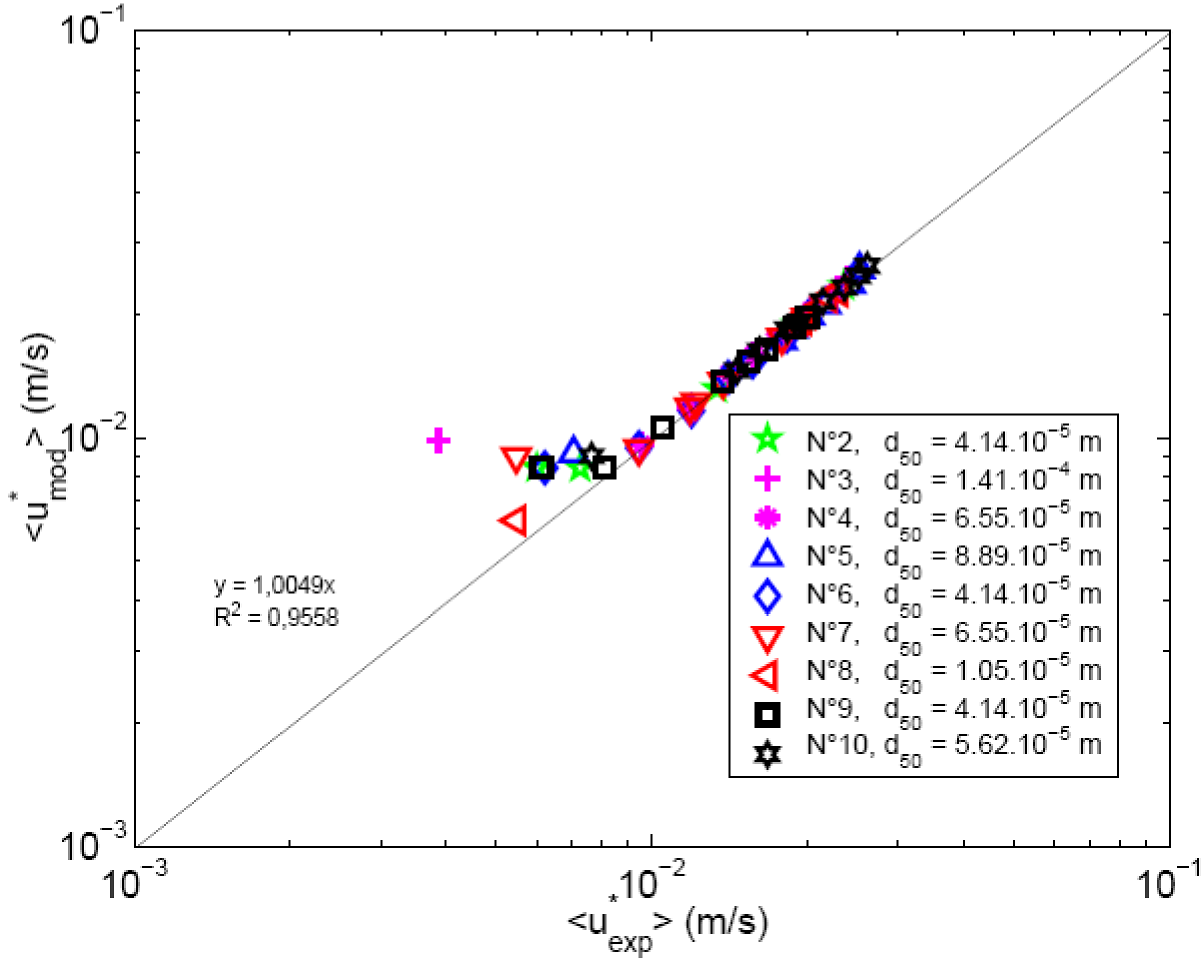

Comparison between experimental and modeled critical erosion velocities u^*_{ce} for all resuspension campaigns.

Conclusion

- The water channel HERODE allowed us to perform experiments on the erosion properties (τ_{ce}, porosity, granulometry) of cohesive sediment
- These results were used as a basis for developing a model of cohesion

Future developments:

- Test the cohesion model on other cohesive sediment (with different origins : different clay contents, different water salinities, different water pH values, …., and different erosion modes also ?)
- Improve the water channel in order to have a better control of the eroded sediment height and of the fraction of saltating eroded matter

Thank you …..